GCM HINDCASTS OF SST FORCED CLIMATE VARIABILITY OVER AGRICULTURALLY INTENSIVE REGIONS

LEONARD M. DRUYAN[1,2], KATHRYN P. SHAH[1,2], MARK A. CHANDLER[1,2] and DAVID RIND[1]

[1]*NASA/Goddard Institute for Space Studies, 2880 Broadway, New York 10025, U.S.A.*
[2]*Center for Climate Systems Research, Columbia University, New York 10025, U.S.A.*

Abstract. The NASA/Goddard Institute for Space Studies (GISS) climate model is forced with globally observed sea-surface temperatures (SST) in five simulations, 1969–1991, with individual runs beginning from altered initial atmospheric conditions. The interannual variability of modeled anomalies of the Southern Oscillation Index, mid-tropospheric temperatures, 850 mb zonal winds and Outgoing Longwave Radiation over the tropical Pacific Ocean, which has the largest SST anomaly forcing, are strongly correlated with observed trends which reflect ENSO cycles. The model's rainfall variability over three agriculturally intensive regions, two tropical and one mid-latitude, is investigated in order to evaluate the potential usefulness of GCM predictions for agricultural planning. The correct sign of Zimbabwe seasonal precipitation anomalies was hindcast within a useful range of consensus only for select seasons corresponding to extreme ENSO events for which anomalous circulation patterns were rather realistically simulated. The correlation between hindcasts of Nordeste monthly precipitation and observations increases with time smoothing, reaching 0.64 for 5-month running means. Consensus between individual runs is directly proportional to the absolute value of Niño3 SST so that during El Niño and La Niña years most simulations agree on the sign of predicted Nordeste rainfall anomalies. We show that during selected seasons the upper tropospheric divergent circulation and near surface meridional displacements of the ITCZ are realistically represented by the ensemble mean of the simulations. This realistic simulation of both the synoptic mechanisms and the resulting precipitation changes increases confidence in the GCM's potential for seasonal climate prediction.

1. Introduction

The ability to forecast seasonal climate is of great practical interest. One of the most obvious benefits would be agriculture, for which various preparations (planting, machinery, irrigation, manpower) would be enabled. The expectation of being able to make such forecasts far enough in advance (on the order of 9 months) hinges on components of the system with the longest persistence or predictability. The mixed results of El Niño forecasts has raised the hope that tropical Pacific sea surface temperatures (SST) fall into this category.

For agriculturally-relevant forecasts to be made, and utilized, requires several conditions. The SST in the regions that affect agricultural areas must be forecast successfully, many months in advance. The climate response to such sea surface temperatures must then be ascertained, either through the use of historical empir-

Climatic Change **45:** 279–322, 2000.

ical studies or models (e.g., GCMs). For practical applications, the agricultural production must be strongly influenced by climate, and farmers on either the local level or through commercial concerns must be able to adjust to using such forecasts.

In a continuing series of papers, we will explore each of these components. This article concerns the question of utilizing SST to forecast the climate in several regions of agricultural production. We optimize the possibility of doing so successfully by using observed SST in a hindcast mode (i.e., a perfect forecast), and we also use the globally observed values (rather than just those from the tropical Pacific, for which predictability has been shown). This then is the ideal situation; in subsequent papers we will explore degrading the results by using only tropical Pacific SSTs, and then using only forecast values from that region. The ultimate goal of the project is to draw some conclusions about how practical forecasts will really be.

With the given set of SST boundary conditions, an ensemble of simulations is performed in an attempt to sample the probability space of the model (and real world) occurrences. Model simulations are based on the solution of the standard Navier–Stokes equations governing fluid flow. A property of these nonlinear equations (and presumably the real world) is that slight variations in the initial conditions lead to much larger differences in the solutions as time progresses. Simulations with different initial conditions produce somewhat different results, but all are indicative of the model's response to any particular boundary condition forcing, such as sea surface temperatures. Hence to get an appropriate estimate of the range of model results, we vary the atmospheric initial conditions, keeping the same initial soil moisture, and run the simulations with the same SST forcing numerous times. It is this range of results which is then compared to the real world 'simulation', which of course has only one realization with a specific atmospheric initial state. Variations among the model runs help define the natural variability (standard deviation) of the model to the initial conditions; if the real world differs from the model mean by more than two standard deviations, it can be thought of as significantly different (with only a 5% chance that the real world occurrence is from the same sample but is simply an outlier).

In the following section we discuss the model used, the set-up of the experiments, and the agricultural regions which are the focus of this work. In the results section we first analyze the broad patterns of model and observed response, and then relate these to the local climate in the agricultural regions. In the discussion section we comment on whether the model simulations, including the variability of the results, would have been useful for agricultural purposes, and what the real world response was in relation to the modeled possibilities.

2. Experiments

While it is possible to use historical empirical relationships to relate El Niño indices to climate in various regions of the world, such an approach assumes that each El Niño produces a similar response regardless of its precise character. The danger in this has been clearly displayed for the El Niño of 1997/1998. Historical relationships indicate that El Niños should be associated with severe drought conditions in portions of Africa, such as Zimbabwe. Yet during this past El Niño, arguably the strongest this century, no widespread drought occurred, and some regions received copious amounts of rain. While no correlative technique can be expected to be perfect, there are physical reasons to suppose that the pattern and strength of El Niños should influence the resulting climate. Therefore, our approach is to use an atmospheric GCM to provide the connection between potentially forecast SST and agriculturally important climate responses.

The GCM used is a version of the GISS Model II', referred to as SI97 to indicate that it incorporates model adaptations frozen for the 1997 'Summer Institute' at GISS. Results from previous versions have been given by Druyan et al. (1995), Rind and Lerner (1996), and Hansen et al. (1997). The model uses a $4^\circ \times 5^\circ$ horizontal resolution with 9 layers in the vertical. A fourth order scheme is used for momentum advection, and a quadratic upstream scheme for heat and moisture advection; these processes allow the model to provide effectively increased horizontal and vertical resolution for numerical advection. Relative to the GCM discussed in Hansen et al. (1983, 'model II'), new physics includes the land surface scheme of Rosenzweig and Abramopolous (1997), new convection and cloud liquid water schemes (Del Genio and Yao, 1993; Del Genio et al., 1996), and a new boundary layer formulation (Hartke and Rind, 1997). A more complete discussion of these various components and their influence can be found in the individual papers and in Rind and Lerner (1996).

The grid resolution being employed here ($4^\circ \times 5^\circ \times 9$ levels) is not as fine as in some other models. Nevertheless, compared with other models run in the AMIP intercomparisons, the model performs quite well, especially with regards to precipitation, of paramount importance in agricultural forecasts. For example, Lau et al. (1996) found that the GISS model was ranked approximately fifth out of 28 GCMs in its ability to simulate components of the hydrologic cycle. Boyle (1998), in assessing the AMIP models' seasonal precipitation cycle, noted that 'a model with low resolution such as GISS appears to perform better than models with more than double the number of grid points'. They concluded that 'the MPI model [with finer horizontal resolution and double the number of vertical levels] and GISS have distributions of precipitation through the year that match the observations fairly well and that match each other'. Given the need for multiple simulations of 30+ years anticipated through the course of this project, it therefore seemed reasonable to utilize this version of the GCM in our initial set of simulations. Other versions of the model exist, i.e., versions including a more sophisticated, second

order closure boundary layer, higher vertical and finer horizontal resolution. In another publication we will explore whether these results can be improved with such additions to the GCM.

The experiments discussed here evaluate the GCM's responses to prescribed observed global sea surface temperatures (SSTs) specified monthly over the time period 1969–1991. The prescribed SSTs are from the analysis of Reynolds and Smith (1994). Those data, originally distributed at $2^\circ \times 2^\circ$ horizontal resolution were interpolated to the GISS GCM's $4^\circ \times 5^\circ$ fractional land/ocean grid using the ETOPO5 data set as a reference for land cover. Sea ice is problematical, and we chose to use a climatological sea ice based on the period 1979–1993 which was modified from the data sets distributed for use with AMIP (Gates, 1992). In a subsequent publication we will explore the separate issue of how transient sea ice change affects the results described here.

Each simulation in our ensemble of five 23-year simulations was initiated using a unique perturbation of the atmospheric state in order to gauge the model's range of responses to arbitrary differences initial conditions. Each of the five simulations, from slightly altered initial conditions, was forced by identical observed SSTs. Simulations are validated against evidence from observed climate variables. Results shown below indicate the 5-run ensemble mean response, and the variability between the individual realizations is discussed as well.

The possibility arises that an ensemble of five simulations may not be sufficient to properly characterize the range of model results, or the model natural variability. However, we can make use of an additional archived set of model runs with 10 simulations, and see how the results for the regions of interest compare with using only five runs. We will show that where the model most properly simulates the observed climate signal, five simulations produce similar results to the full 10; where the model fails to provide a meaningful signal in five runs, 10 simulations does not help. This 'either/or' character of the model's success in forecasting for agricultural regions thus allows five simulations to be sufficient for the detailed analysis. The results might well be different for regions where the model's results are of marginal significance, as is often the case in general seasonal forecasting.

Many countries produce important agricultural products, and it is not feasible for us to investigate all of them. The project's focus therefore is on regions for which there is reason to believe, from empirical studies, that sea surface temperature variations (in particular El Niños) are likely to have an influence. The present paper presents results for two low latitude regions directly affected by altered tropical circulations, and one mid latitude region of importance, to include extratropical teleconnections. The regions are: Zimbabwe (whose location falls in GCM grid boxes which span 16–24° S, 22.5–32.5° E); Nordeste (4°–12° S, 37°–48° W); the U.S. corn belt (36–44° N, 87.5–97.5° W). We first discuss the realism of the simulations in the broadest terms, the planetary scale.

3. Tropospheric Temperature Structure

The GCM's tropospheric temperature structure was validated against microwave sounding unit (MSU) brightness temperatures (Tb) via a microwave radiative transfer postprocessor. This microwave model calculates the Tb which would be measured by the satellite-borne MSU if it observed the simulated GCM climate. Previous applications of MSU Tb climatologies as useful validation datasets of climate models are described by Shah and Rind (1995, 1998), Druyan et al. (1995) and Rind et al. (1998). MSU monthly-means over 1982–1991 and anomalies over 1979–1992 are used to examine the GCM's mean annual cycle and regional interannual variability. Departures from the observed tropospheric temperature structure imply deficiencies in GCM-simulated tropospheric humidities, evaporation and precipitation, vertical stability and other coupled physical processes.

The MSU measures temperatures over broad layers centered in the lower troposphere (800 mb), the mid-troposphere (600 mb), the upper troposphere (270 mb) and the lower stratosphere (80 mb) in channels labeled 2R, 2, 3R and 4 respectively. The current MSU channels, 2 (53.74 GHz), 3 (54.96 GHz), and 4 (57.95 GHz), are radiances from 200 MHz bandwidths on the low-frequency side of the 60 GHz molecular oxygen band. MSU Tb measure atmospheric temperatures and, for tropospheric channels, surface-emissivity weighted skin temperatures. Microwave temperatures are thus quite sensitive to the underlying surface's emissivity and mid-tropospheric channel 2 derives roughly 10% of its full signal from land-surface emission (Shah and Rind, 1995). Atmospheric humidity is a much more minor influence on MSU tropospheric values, adding an opacity to channel 2 Tb which either cools over a land backdrop or warms over an ocean backdrop by up to 0.5 K across near-equatorial latitudes (Shah and Rind, 1995). All of the MSU channels are nearly insensitive to the presence of non-precipitating clouds (Shah et al., 1996; Shah and Rind, 1995). The more variable and less significant opacity from cloud liquid water was quantified with a full Mie scattering code (A. Lacis, personal communication) and cloud characteristics from the International Satellite Cloud Climatology Project (ISCCP) (Rossow and Schiffer, 1991). Precipitation influences, which can cool Tb values by several degrees, were filtered from the MSU data (Spencer and Christy, 1992). Current uncertainty regarding tropospheric aerosols' size, composition and distribution make an assessment of their impact on channel 2 Tb difficult at best, but their short residence time and usually low altitude minimize the problem.

Overall, the 10-year average, 1982–1991, of monthly GCM variables produced mean Tb values in reasonable agreement with the MSU mean climatology. Simulated tropospheric temperatures were 2–6 °C too cool over the mid-to-high latitudes, especially during the summer season. Also, the GCM's lower tropospheric Tb were significantly too cool (based on ratios to MSU interannual standard deviations) by roughly 2 °C across equatorial oceans and some 5 °C across high

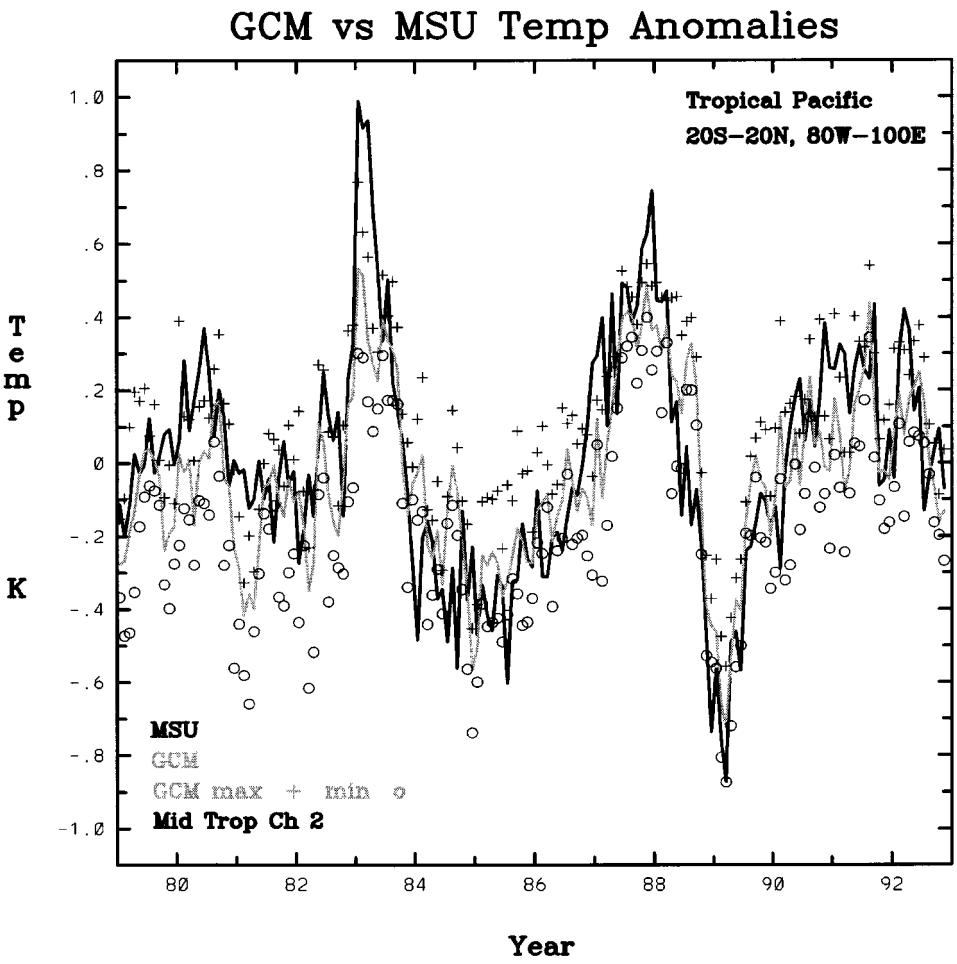

Figure 1. Mid-tropospheric monthly temperature anomalies over the Tropical Pacific Ocean (20° S–20° N, 100° E–80° W) for the ensemble average of five model simulations (gray, relative to 1969–1992) and MSU observations (black). The highest (+) and lowest (○) of the five simulated values for each month are indicated.

latitude oceans. This may be related to insufficient high cloud coverage in the GCM's northern latitudes and to atmospheric moisture levels which are difficult to confirm. However, such tropospheric temperature deviations are common flaws in AGCMs (Boer et al., 1992; Houghton et al., 1996).

The temporal variability of simulated temperatures was realistically higher over high latitudes, winter seasons, and continents. However the magnitude of this variability was too weak, peak values being only about half of those measured by MSU.

Since ENSO cycles dominate tropospheric temperature variability and since these GCM runs were forced only by observed SSTs, one expects best agreement

between the observed and modeled tropospheric Tb variability over the tropical Pacific basin (20° S–20° N, 80° W–100° E). Indeed, appropriate warming of GCM channel 2, mid-tropospheric Tb did occur due to El Niño events in the 1980s (see Figure 1). The GCM's sensitivity to its initial state produced a range of tropospheric temperature responses, which in turn, could prompt a range of teleconnections to the extratropics. Over the tropical Pacific, correlation coefficients of the individual simulations with MSU channel 2 time series range from 0.66 to 0.74. The ensemble mean of the five runs produced a consensus of mid-tropospheric Tb which were better correlated with MSU Tb than any individual run ($r = 0.78$). The ENSO tropical temperature response is zonally quite uniform across the tropics (Yulaeva and Wallace, 1994), unlike OLR anomalies or 850 mb wind field anomalies (discussed below). Consequently, the temporal correlations between modeled and observed Tb were somewhat higher over the entire zonal band 20° S–20° N (ensemble $r = 0.82$). Smoothing of GCM and MSU Tb time series with 3-month filters and with 5-month filters improved the ensemble correlation coefficients to 0.85 and 0.88 respectively over the tropical Pacific, demonstrating the GCM's skill in capturing the low frequency signal. Correlations between model temperature simulations and observations may improve further with future GCM runs that include other known, observed climate forcings: trace gases, stratospheric ozone loss, stratospheric volcanic aerosol loading and the QBO. In addition, a stronger ENSO signal from the new AMIP II SST (Hoerling and Kumar, 1997) may additionally improve the model's overall response to SST forcing.

4. SOI and ENSO Variability

Since the interannual variability of SST over this time frame is dominated by the occurrence of El Niños, ascertaining the model's tropical response is of first order importance. The variation of the Southern Oscillation Index (SOI) is one reasonable measure of the tropical atmosphere's response to strong SST forcing. Since it is computed as the Tahiti minus Darwin difference in sea-level pressure, it also represents a rather local response to the ENSO cycle, whose largest SST oscillations are in the tropical Pacific Ocean. A high correlation between SST-forced simulations of SOI and observations is probably a minimum requirement for success in simulating more remote climate responses.

Figure 2 shows the observed SOI anomalies for 1969–1991 compared with the modeled SOI for the five simulations. Negative SOI coincides with warm (El Niño) episodes in the central/eastern tropical Pacific, and these are prominent during 1972, 1977, 1982–1983 and 1987. Positive anomalies that peak during cold tropical Pacific SST episodes are apparent during 1971, 1973–1974, 1975 and 1988-1989. While modeled SOI maxima and minima for all of the simulations are mostly less extreme than observed peaks, the simulations show distinctive responses to the ENSO cycles. Variability between the model runs is particularly low in response

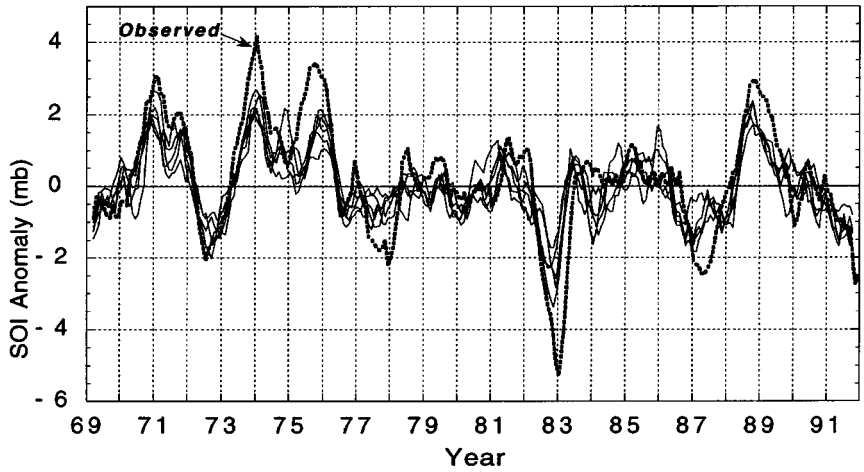

Figure 2. Five-month running means of Southern Oscillation Index (SOI) anomalies. The SOI is computed as the difference in sea-level pressure between the locations, Tahiti minus Darwin. Pressures for the model's SOI are single grid point values and anomalies are computed relative to the base period 1969–1991. The observed SOI (courtesy, Australian Bureau of Meteorology, www.bom.gov.au/climate/current/soihtm1.shtml) is computed relative to the base period 1950–1997.

to the warm ENSO event of 1972 and the cold events of 1973–1974 and 1988-1989. On the other hand, modeled responses to the warm events of 1983 and 1987 indicate a wider rage of amplitudes, although all simulations register SOI anomaly minima. The correlation of the ensemble mean SOI with the observed time series (both represented by 5-month running means) is a highly significant 0.86. The lower amplitudes of simulated SOI extremum, consistent with a similar behavior of Tb (Figure 1), may have implications for more remote model responses to the SST forcing which may be weaker than actual climate variability forced by ENSO.

5. Time-Longitude Cross Sections and ENSO Variability

5.1. ZONAL WIND ANOMALIES, 850 MB

Local circulation responses associated with ENSO include the slackening of south-easterly trade winds along the Pacific Equator during warm El Niño phases and their strengthening during cold phases. We compare the 1971–1991 time-longitude cross sections of NCEP reanalysis (Figure 3a) and simulated (Figure 3b) 850 mb zonal wind anomalies (ΔU_{850}) over the equatorial Pacific Ocean. Each El Niño is characterized by positive (westerly) anomalies over the mid-Pacific, often appearing first in the west and propagating thereafter eastward. Note, for example, the positive ΔU_{850} anomaly over the western third of the Pacific in 1982 which strengthened as it moved eastward, reaching 6–8 m sec^{-1} later in the year over the Central Equatorial Pacific (see also Kousky and Leetmaa, 1989). During the

first half of 1983, the positive ΔU_{850} anomaly approached the South American coast, while negative (easterly) anomalies appeared over the western Pacific. This evolution traces a distinctive diagonal pattern on the time-longitude cross section which is easily compared to model results.

This wind anomaly propagation is a first order response of the modeled circulation to SST forcing in the Pacific. It is not likely that realistic circulation responses affecting more remote regions could be correctly simulated if this in situ response were badly handled. Model ensemble mean ΔU_{850} (Figure 3b) were indeed positive during the El Niño episodes of 1972, 1983, 1987 and 1991. Moreover the characteristic diagonal patterns of the first two episodes are captured in the simulations, showing very realistic timing in the development of the westerly anomalies and their replacement by easterlies. The observed appearance of positive ΔU_{850} in the west in January 1986 and their eventual propagation to the Central Equatorial Pacific during the 1987 El Niño was also captured by the simulations. The correlation coefficient between these observed and modeled time series of ΔU_{850}, averaged over 135° E–180°, is a highly significant 0.81 (Figure 3c). In general, modeled ΔU_{850} have a smaller range than observed, consistent with the smaller range of modeled SOI and Tb oscillations.

5.2. OUTGOING LONGWAVE RADIATION ANOMALIES

Outgoing long-wave radiation anomalies (OLRA) assume extreme negative values above the towering convective towers of the tropics. Strongly negative monthly mean OLRA at tropical latitudes indicate regions with frequent heavy convective precipitation. Kousky and Leetmaa (1989) represented OLRA over the Equatorial Pacific on a time-longitude cross section for July 1981–January 1988 and showed that negative OLRA propagate eastward across the Equatorial Pacific during an El Niño, in tandem with the positive ΔU_{850} (Figure 3). This pattern relates to the appearance of warm SST anomalies which destabilize the lower troposphere and trigger more frequent convective events than on average. Simulation of the OLRA pattern therefore requires realistic modeling of the air-sea energy exchange, moist convection and other dynamic feedbacks to the convection from additional atmospheric processes related to the ENSO cycle.

OLRA from NCEP reanalyses (Figure 4a) underwent cycles of waxing and waning convection over the Equatorial Pacific which are a reasonable match with the shorter record of satellite observed OLRA patterns (Figure 4b) during the years that these data overlap. OLRA from the ensemble mean simulation (Figure 4c) capture the essence of this observed spatial and temporal variability, more so over the Central Equatorial Pacific than over the western or eastern margins. We note in particular the large OLRA minimum corresponding to anomalously heavy rainfall during the El Niños of 1972 and 1982–1983 as well as a less extreme episode during 1987. In each case OLRA minima were simulated reasonably well with respect to location and timing as was the 1984–1986 hiatus in organized and sustained

moist convection over the Central Equatorial Pacific. The ensemble of simulations also shows close agreement regarding a similar break in moist convective activity corresponding to a very strong La Niña during 1988–1989.

6. Regions

Simulated precipitation rates are discussed for three selected regions: Zimbabwe, Northeast Brazil (Nordeste) and the U.S. Corn Belt.

6.1. ZIMBABWE (16–24° S, 22.5–32.5° E)

6.1.1. *Background*

Rainfall in Zimbabwe is very seasonal, peaking around January in synchrony with the location of the ITCZ over the region. Five contiguous months, November–March, experience the most significant rainfall, usually accounting for 80–90% of 12-month accumulations.

Based on data from the beginning of the century, Matarira (1990) associated eleven out of sixteen cold tropical Pacific SST events with above normal rainfall in Zimbabwe and fourteen out of nineteen warm SST (El Niño) events with rainfall deficits. Moreover, between 1900–1992, 86% of all Zimbabwe seasons experiencing rainfall departures larger than one standard deviation from the mean coincided with extreme phases of the SOI (Makarau and Jury, 1997).

Matarira (1990) computed correlations between time series of November–April precipitation totals at individual Zimbabwe stations and the annual mean SOI (previous January–December). Values ranged from near zero to a high of 0.42. The spatial orientation of the region of largest correlations suggests that the Southern Oscillation (SO) modulates the activity of major rain-producing synoptic systems within a northwest-southeast swath across Zimbabwe. Both Matarira (1990) and Lindesay (1988) refer to eastward moving northwest – southeast oriented troughs

Figure 3 (facing page). Time-longitude distributions of zonal wind component anomalies at 850 mb (Δu) between 1971–1991 averaged over 5° S–5° N between 100° E–80° W (ms^{-1}). Left: NCEP reanalysis (courtesy, Climate Diagnostics Center, www.cdc.noaa.gov/ncep_reanalysis.); right: model ensemble means; bottom: time series of 5-month running means of modeled versus NCEP Δu (ms^{-1}) between 1979–1991 averaged over the longitudinal band 135° E–180°.

Figure 4 (facing page). Time-longitude distributions of Outgoing Longwave Radiation anomalies averaged over 5° S–5° N between 100° E–80° W (Wm^{-2}). Left: NCEP reanalysis (courtesy, Climate Diagnostics Center, www.cdc.noaa.gov/ncep_reanalysis.); middle: satellite observed (Courtesy of Climate Diagnostics Center, www.cdc.noaa.gov/Public Data/.); right: model ensemble means.

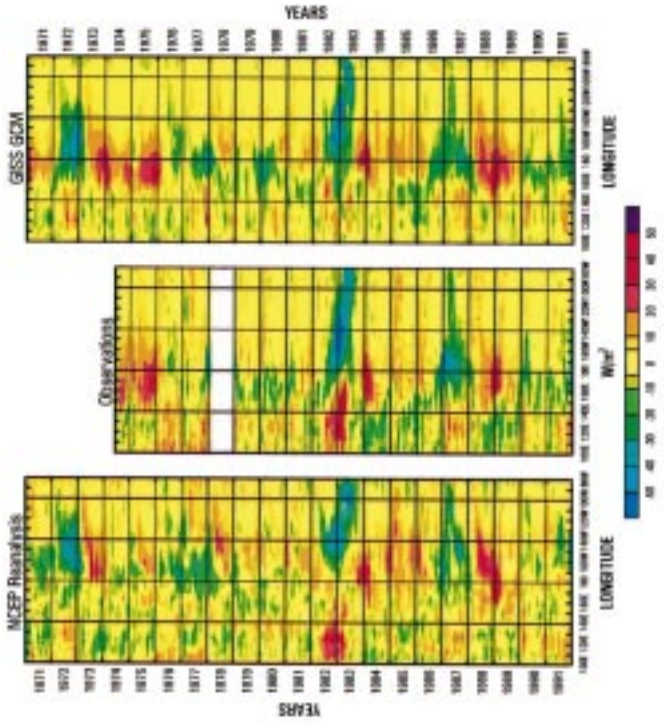

Figure 4

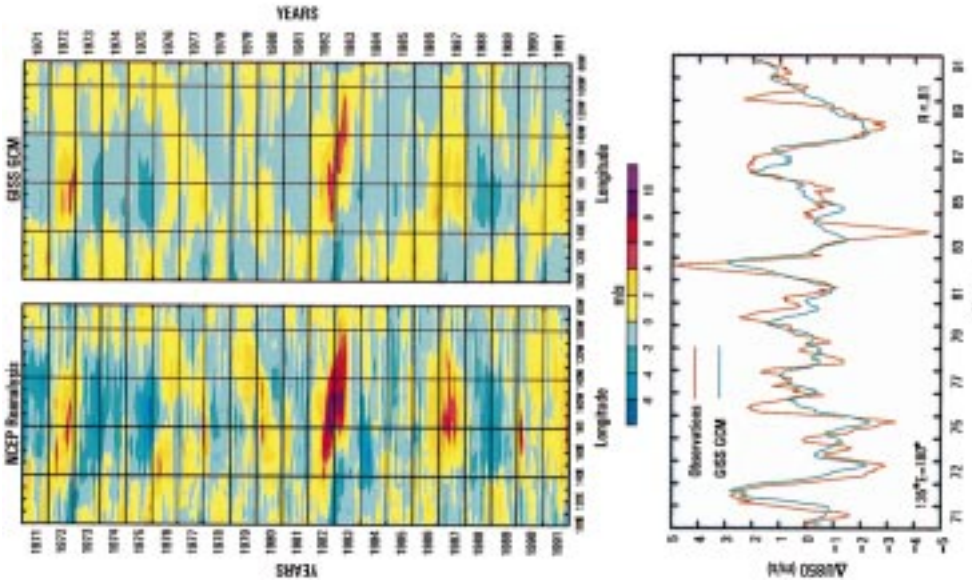

Figure 3

as being among the major determinants of Zimbabwe rainfall anomalies. Such troughs connect tropical systems over central southern Africa with mid-latitude depressions south of the subcontinent. Indeed, anomalously low sea-level pressure during the wet years enhances moisture convergence over the region while the opposite occurs during dry seasons associated with Pacific warm events (Matarira, 1990). Lindesay (1988) suggested that the low phase of the SO (El Niño) coincides with an eastward shift of convection areas related to the Walker circulation around much of the tropical belt, and thus rain-producing cloud bands are displaced (eastward) toward Madagascar and the Indian Ocean during these years. It is nevertheless important to emphasize that all of the studies to date have found that the ENSO cycle explains only a small portion of the Zimbabwe interannual rainfall variability (Makarau and Jury, 1997). Land surface conditions, SST anomalies outside the tropical Pacific, interactions with other regional and planetary circulations and inherent atmospheric variability must additionally be considered to account for more of the Zimbabwe rainfall variability. GCM simulations, of course, include all of these influences.

The time-mean spatial distribution of GCM simulated precipitation is quite reasonable. Figure 5 compares the global distribution of modeled January (23-year) mean precipitation rates to observations analyzed by Legates and Willmott (1990). Of particular relevance here is the realistic GCM representation of the January maximum across southern Africa, oriented northwest/southeast from Zaire to Madagasgar, as well as the modeled pattern of ITCZ/monsoon precipitation maxima in the Indian Ocean and the southwest Pacific that also compares well to observational evidence.

6.1.2. *Time Series*

Figure 6 shows the November–March observed precipitation anomalies (relative to the base years, 1969–1991) for the 22 seasons covered by the GCM experiments. Simulation ensemble mean November–March anomalies (relative to the GCM 22-year mean) are compared to the corresponding observations in Figure 6, and the standard deviation (σ) between the five model runs is also indicated.

The observations show seven droughts for which Zimbabwe experienced seasonal deficits of more than 100 mm; two of these deficits were more than 200 mm.

GCM simulated anomalies are less extreme than observed, in part owing to the averaging of results from five simulations. The correlation coefficient between the ensemble means and the observations shown in Figure 6 is only 0.23, not statistically significant. Model results indicate relative minima for four of the seven droughts, but the large range of results over the five simulations (implied by σ) for two of these seasons suggests that the SST forcing was not decisive. The two 'reasonable' hindcasts, 1972–1973 and 1982–1983, may not be the consequence of pure chance since these *are* the driest seasons observed in Zimbabwe during the 22-year interval. Moreover, both dry extremes coincide with warm El Niño episodes.

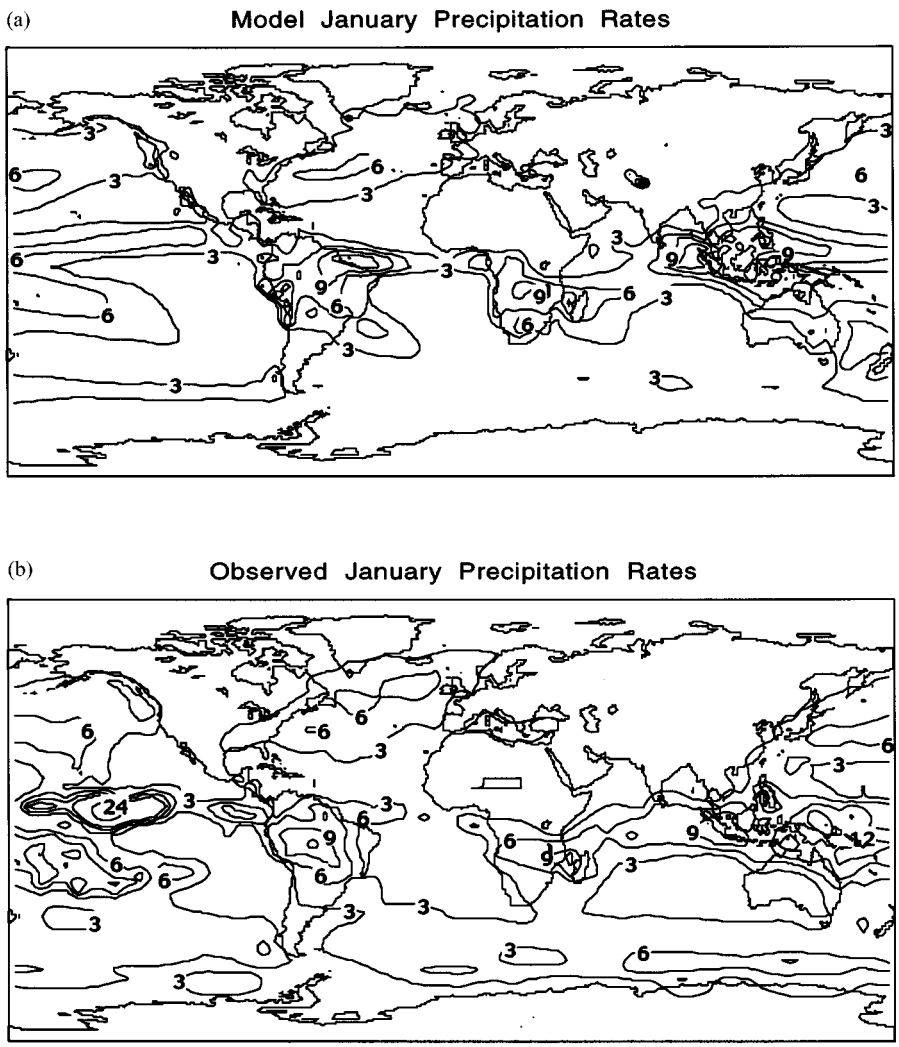

Figure 5. January mean precipitation rates (mm day^{-1}): (a) 23-year model mean; (b) Observed (Legates and Willmott, 1990).

In addition, during the strong La Niña episode of November–March 1972–1973, Zimbabwe experienced one of its rainiest periods. Figure 6 shows that the model ensemble hindcast for this season is a modest positive anomaly, with three of the five simulations supporting that response.

We cannot demonstrate the statistical significance of the GCM hindcasts of drought for 1972–1973 and 1982–1983 since the 22-year correlation between model and observations was small. However, because the agreement was achieved

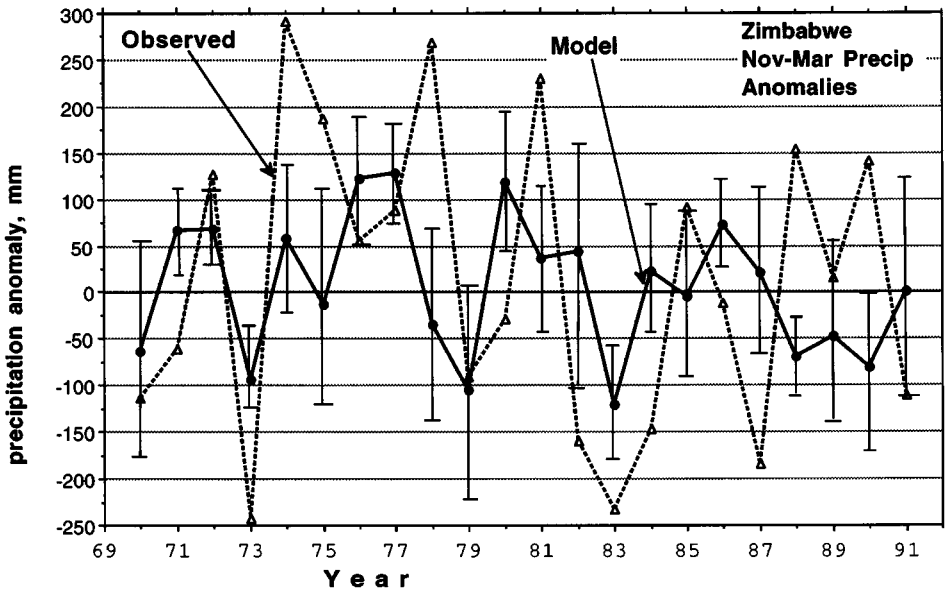

Figure 6. Time series of November–March precipitation anomalies (mm) for Zimbabwe. Broken line: Area average based on station observations relative to 1969–1991. Solid line: Ensemble mean of five GCM simulations relative to 1970–1991, for grid boxes bounded by 16–24° S, 22.5–32.5° E. Vertical bars indicate the standard deviations between the five simulations.

for seasons with well organized large SST anomalies, these hindcasts may be representative of the limited GCM sensitivity to a Zimbabwe-SST teleconnection.

We note also that there was consensus on a positive anomaly for November–March 1972, evidenced by $\sigma = 80$ mm between the GCM ensemble members. Observations indicate that a positive anomaly for this season was a reasonable hindcast. Referring to Figure 6, nine hindcasts of the November–March ensemble mean precipitation anomaly out of the 22 seasons that were evaluated validated with the correct sign, but for only five or six of these was σ sufficiently small to suggest any consensus.

6.1.3. *Analysis of Selected Seasons – Planetary Circulation*

Figure 7a shows the velocity potential for the simulated 200 mb wind field (χ_2) of the DJF 1972–1973 La Niña season. These χ_2 patterns exhibit several important departures from the mean field of the 22-year simulation (Figure 7b). The center of negative χ_2 normally over the maritime continent during DJF represents the focus of convection associated with the rising branch of the Pacific Walker circulation. Maxima over the South Atlantic and Southeastern Pacific mark regions of broad-scale subsidence. During the El Niño of DJF 1972–1973, the modeled upper tropospheric divergence associated with the convection over Indonesia was weaker and more diffuse, as evidenced by the positive χ_2 anomalies (with respect to the 22-year mean distribution) shown in Figure 7c. Moreover, the area

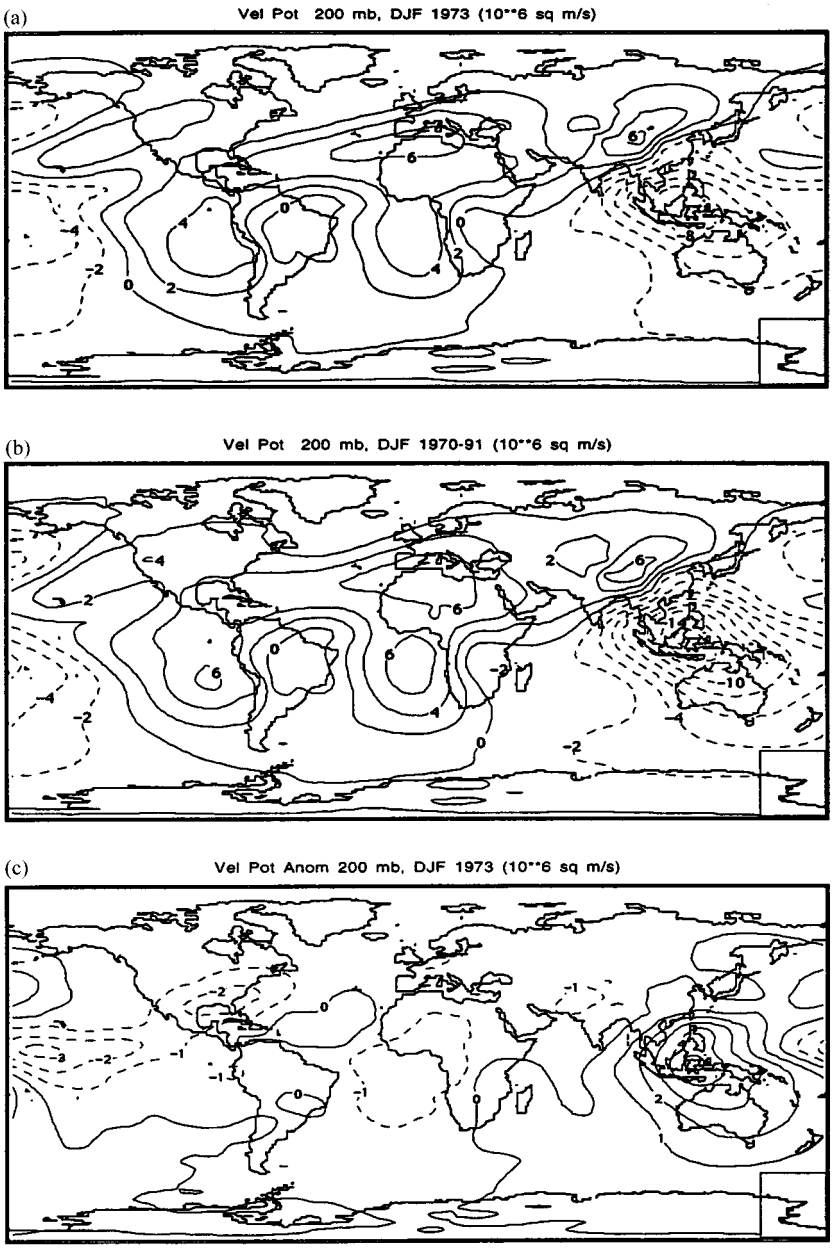
(a)
Vel Pot 200 mb, DJF 1973 (10**6 sq m/s)
(b)
Vel Pot 200 mb, DJF 1970-91 (10**6 sq m/s)
(c)
Vel Pot Anom 200 mb, DJF 1973 (10**6 sq m/s)

Figure 7a–c.

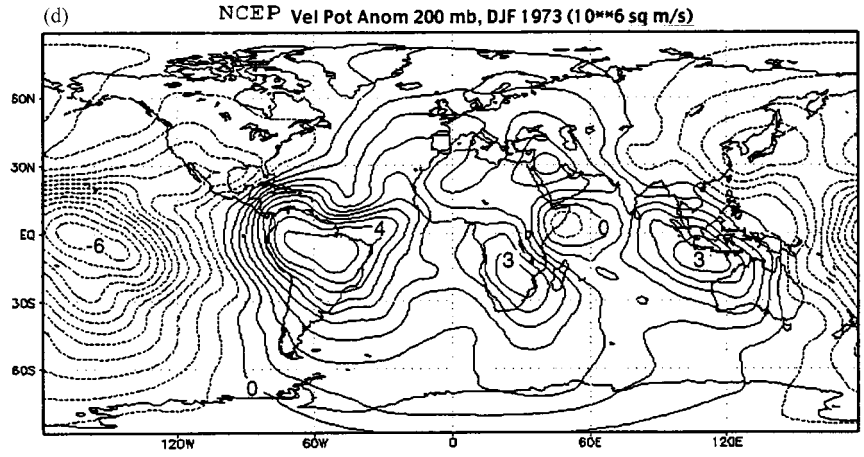

Figure 7d.

Figure 7. Velocity potential of the 200 mb winds (10^6 m^2 s^{-1}): (a) GCM ensemble for December 1972–February 1973; (b) GCM ensemble for December–February, 1970–1991; (c) GCM anomalies for December 1972–February 1973, (a) minus (b); (d) NCEP observed anomalies (relative to 1958–1997) for December 1972–February 1973. (Courtesy of Climate Diagnostics Center, www.cdc.noaa.gov/ncep_reanalysis.)

of upper tropospheric divergence was also expanded eastward toward Mexico, presumably a result of the warm SST anomalies in the eastern Pacific which enhanced convection.

The NCEP reanalysis χ_2 anomaly field for DJF 1972–1973 (Figure 7d) features positive centers over South Africa, South America and the Maritime Continent (centered on Indonesia), all indicative of diminished convective activity. The major negative center is over the eastern tropical Pacific Ocean, presumably a response to the warm SST anomalies of this El Niño season which enhance deep convection. We also note the relative minimum (χ_2 anomaly) over the western Indian Ocean, which indicates that the weakening of convection over South Africa was not spatially contiguous with the similar tendency within the Asian–Australian monsoon system. Modeled χ_2 anomalies (Figure 7c) reflect the observed El Niño induced changes in circulation over the Pacific Ocean and over the Asian–Australian monsoon region. However, the model ensemble did not produce the positive center that the NCEP reanalysis showed over South America and the South Atlantic. Moreover, the modeled minimum over the Central Pacific Ocean was weaker than analyzed (Figure 7d). Over Zimbabwe, modeled χ_2 anomalies for DJF 1972–1973 were slightly positive, and over the western Indian Ocean, slightly negative. In both the simulations and the real world, we presume that the shallower troughing (hence weaker upper tropospheric divergence) over southern Africa during DJF 1972–1973 contributed to less intense rainmaking systems within the ITCZ.

The spatial distribution of large scale vertical motion can also be monitored in NCEP reanalyses (not shown). The multi-year mean circulation for DJF over Zimbabwe includes uplift throughout the troposphere, with the axis of maximum values along a sloping surface from the lower troposphere near 25° S to about 300 mb over northern Zimbabwe near 15° S. The anomalously dry season DJF 1972–1973 experienced large scale subsidence over Zimbabwe within the upper half of the troposphere undoubtedly inhibiting deep moist convection, as did the weaker than normal uplift between 900–700 mb. Although the vertical motion field was slightly more favorable for convection during the very pronounced El Niño DJF 1982–1983, there was still some subsidence aloft over southern Zimbabwe, and uplift was weaker than normal above 900 mb throughout the troposphere. During both of these anomalously dry seasons the strongest uplift within the upper troposphere was displaced to the northeast of Zimbabwe compared to its climatological mean position.

Other contrasts between the DJF 1982–1983 and DJF 1972–1973 SST-forced anomalous planetary circulations can be discerned. The ensemble simulation for DJF 1982–1983 was somewhat more skillful than DJF 1972–1973 in capturing the main features of the El Niño circulation signature depicted by NCEP reanalyses. Figure 8a shows the eastward shift of negative χ_2 relative to the 22-year mean field (Figure 8b) over the Pacific, the weakened Asian–Australian outflow, sharper troughing of negative χ_2 over the western Indian Ocean and shallower troughing over South Africa. The modeled anomaly field (Figure 8c) therefore includes positive centers over the Maritime Continent, South Africa and South America, and the significant negative center over the eastern tropical Pacific Ocean. An additional negative center over the western Indian Ocean (again) separates weakened convection associated with the Zimbabwe drought from the diminished monsoon convection. The NCEP reanalysis of the DJF 1982–1983 χ_2 anomalies (Figure 8d) validates the locations of these extremum and indicates that their simulated amplitudes were slightly underestimated.

Circulation features simulated for DJF 1973–1974, during a cold phase of the ENSO cycle are represented by the χ_2 analysis in Figure 9a. While the Asian–Australian monsoon is strengthened by stronger outflow (than during the El Niño seasons or the 22-year mean DJF field, Figure 9b), ridging of positive χ_2 over the western Indian Ocean is compatible with co-located weaker convection. Over South Africa, the rather intense χ_2 minimum implies strong upper tropospheric divergence and uplift, even though χ_2 anomalies are positive there (Figure 9c). The simulated χ_2 anomaly pattern for DJF 1973–1974 validates especially well against the corresponding NCEP reanalysis (Figure 9d) over the zone from South America eastward to Australia, although the correspondence over the central and eastern Pacific Ocean is poor. We note that the NCEP reanalysis χ_2 anomaly maxima and minima are opposite in phase from those in the previously cited warm event examples over most of the tropics. The NCEP reanalysis fields for DJF 1973–1974 indicate uplift (not shown) throughout the troposphere over Zimbabwe, with

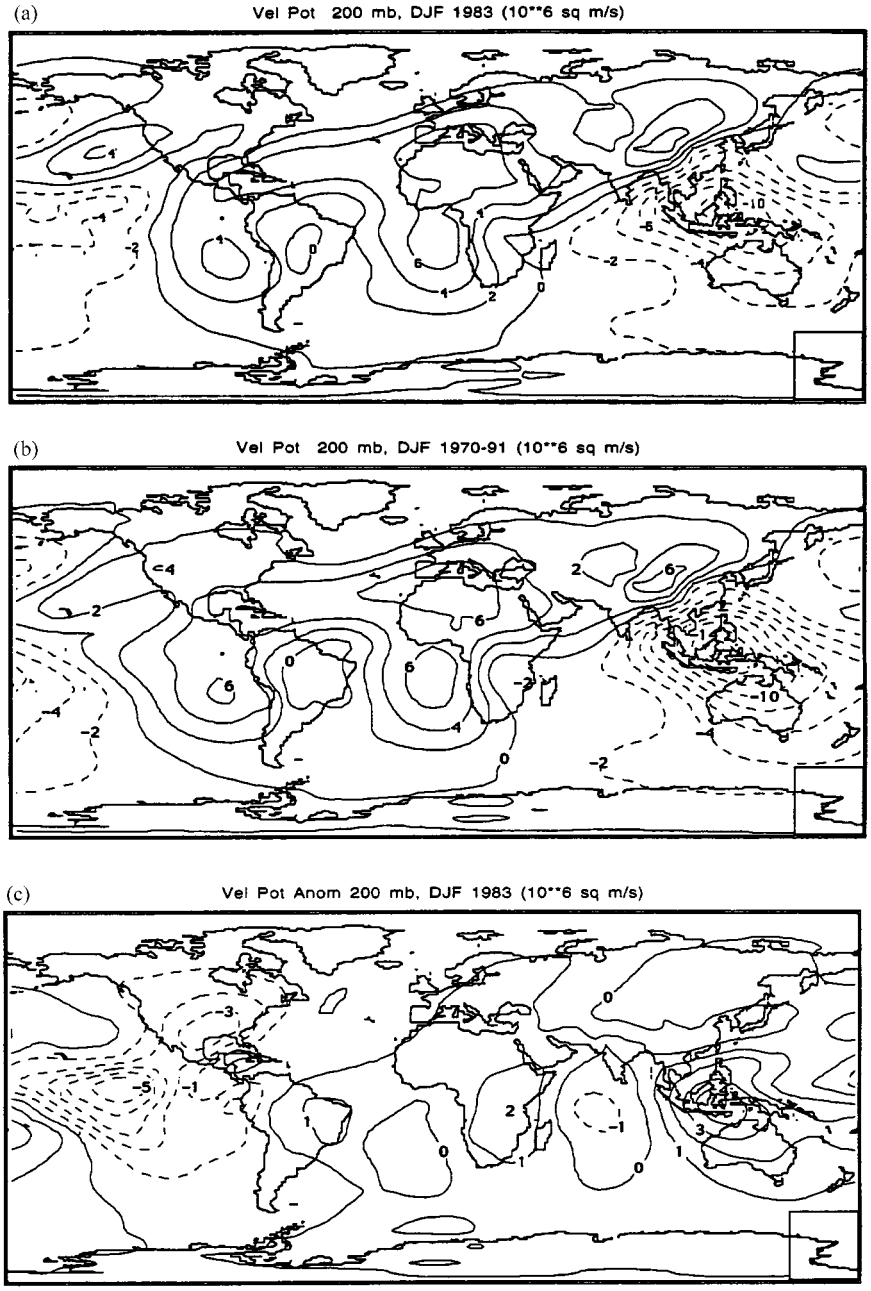
(a)
Vel Pot 200 mb, DJF 1983 (10**6 sq m/s)
(b)
Vel Pot 200 mb, DJF 1970-91 (10**6 sq m/s)
(c)
Vel Pot Anom 200 mb, DJF 1983 (10**6 sq m/s)

Figure 8a–c.

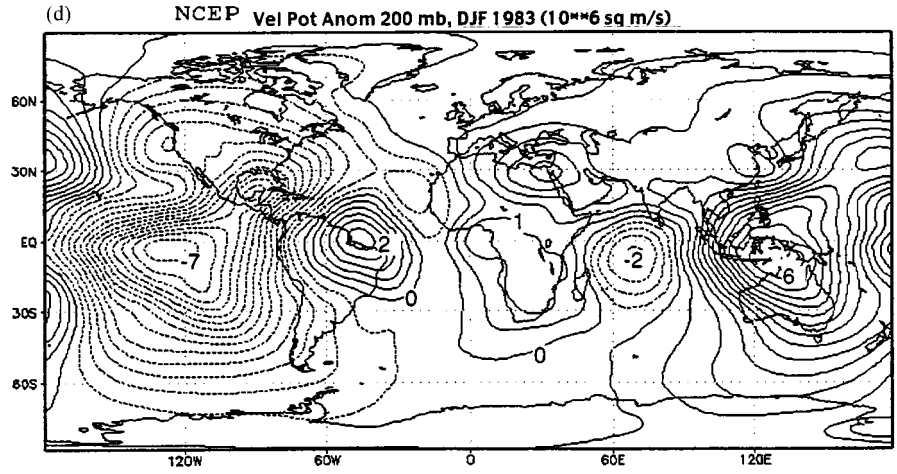

Figure 8d.

Figure 8. Velocity potential of the 200 mb winds (10^6 m^2 s^{-1}): (a) GCM ensemble for December 1982–February 1983; (b) GCM ensemble for December–February, 1970–1991; (c) GCM anomalies for December 1982–February 1983, (a) minus (b); (d) NCEP observed anomalies (relative to 1958–1997) for December 1982–February 1983. (Courtesy of Climate Diagnostics Center, www.cdc.noaa.gov/ncep_reanalysis.)

anomalies favoring more vigorous convection than in the mean, especially between the surface and 700 mb over the southern half of the country. The zone of maximum uplift intersects the surface over southern Zimbabwe in DJF 1973–1974, rather than south of the country as in the DJF 1979–1995 mean field, while an additional region of strong uplift not present in the mean circulation appears within the upper troposphere south of Zimbabwe.

There appears to be an interannual modulation of the intensity of the major tropical convection zones during the austral summer which is sensitive to the ENSO cycle. During (warm phase) El Niño episodes, convection is anomalously stronger over the eastern tropical Pacific and the Indian Ocean and anomalously weak over the region of the Asian–Australian monsoon, South Africa and Brazil. Areas of weakened (strengthened) convection coincide with positive (negative) χ_2 anomalies and weakened (strengthened) uplift. Observed precipitation rates north and east of Zimbabwe (Madagasgar–Tanzania–Zaire) seem to be negatively correlated with rainfall over Zimbabwe itself (Chelliah et al., 1998).

6.1.4. *Analysis of Selected Seasons – Precipitation*

The ensemble mean precipitation distributions for El Niño episodes November 1972 through March 1973 (hereafter Pr73) and Pr83 (Figures 10a,b) have common characteristics over much of the tropics. Over South Africa, the axis of maximum rainfall in both cases is oriented northwest–southeast to the north of Zimbabwe, with rates of less than 6 mm day^{-1} over most of the country. For the La Niña

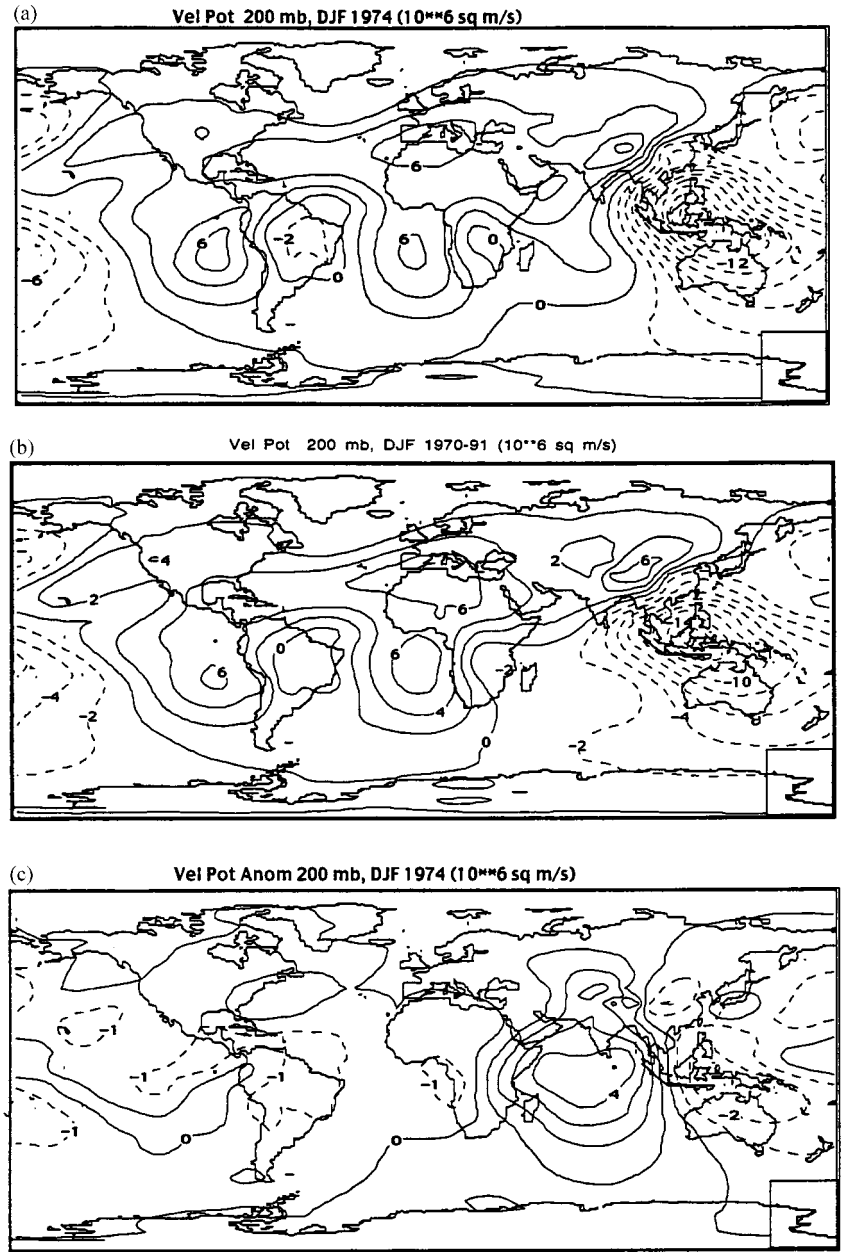
(a)
Vel Pot 200 mb, DJF 1974 (10**6 sq m/s)
(b)
Vel Pot 200 mb, DJF 1970-91 (10**6 sq m/s)
(c)
Vel Pot Anom 200 mb, DJF 1974 (10**6 sq m/s)

Figure 9a–c.

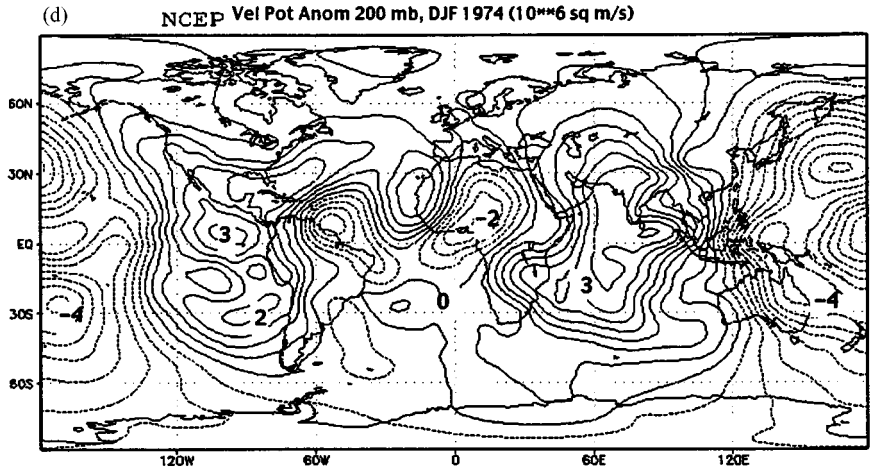

Figure 9d.

Figure 9. Velocity potential of the 200 mb winds (10^6 m^2 s^{-1}): (a) GCM ensemble for December 1973–February 1974; (b) GCM ensemble for December–February, 1970–1991; (c) GCM anomalies for December 1973–February 1974, (a) minus (b); (d) NCEP observed anomalies (relative to 1958–1997) for December 1973–February 1974. (Courtesy of Climate Diagnostics Center, www.cdc.noaa.gov/ncep_reanalysis.)

episode Pr74 (Figure 10c), the axis of maximum precipitation over South Africa has not shifted, but extreme values are somewhat higher, as are rates over Zimbabwe. Precipitation anomaly distributions for these seasons were constructed relative to the 22-year mean rainfall rates for the entire simulation. Anomalies for Pr73 and Pr83 (hereafter Pr73an, Pr83an) shown in Figures 11a,b are strikingly similar to each other in many respects. Each indicates negative values (1–2 mm day^{-1} = 150–300 mm for the season) over Zimbabwe, positive differences over the Indian Ocean and negative differences over the Asian–Australian monsoon region. In addition, the equatorial east Pacific experienced very large modeled excesses in rainfall during both of these seasons, undoubtedly related to the specified positive SST anomalies.

The similarities in the simulated precipitation anomaly fields, Pr73an and Pr83an, over such a wide sector of the tropics lend support to the assumption that the Zimbabwe droughts are related to the El Niño warm events in the Pacific which were common to both years. Indeed, the same pattern of negative and positive areas emerges in December–February precipitation anomaly composites contrasting El Niño warm episodes with La Niña cold events (Chelliah et al., 1998), based on both NCEP reanalyses (12 years) and CAMS_OPI data (six years) published in the Climate Diagnostics Bulletin. Zimbabwe received abundant rainfall during November 1973–March 1974, which coincided with a cold phase of ENSO. Figure 11c shows the Pr74an distribution for which many of the tropical precipitation anomalies are

opposite in sign from those simulated for Pr73an and Pr83an. Pr74an features small positive anomalies over Zimbabwe that contrast with negative anomalies over the Indian Ocean; positive anomalies appear over New Guinea and negative anomalies over much of the equatorial Pacific.

Precipitation anomaly distributions based on rain gauge data show that deficits over South Africa during November 1972–March 1973 were the most widespread during December, within a swath running northwest–southeast through the center of Zimbabwe and Mozambique. The spatial distribution of the ensemble's modest negative anomalies for Pr73an (Figure 11a) is therefore quite realistic in this region, although it lacks a parallel band of enhanced rainfall that was observed through Madagasgar–Tanzania–Zaire. One year later (November 1973–March 1974), observed rainfall anomalies have reversed sign along the Mozambique–Zimbabwe axis indicating abundant precipitation. The ensemble simulation (Figure 11c) shows a similar indication, except at a somewhat reduced magnitude. The observed precipitation anomaly distributions for December 1982 and January 1983 also validate the southeast-northwest oriented area of hindcast negative anomalies for Pr83an shown in Figure 11b.

Satellite observed OLR distributions reflect the spatial distribution of convective rainfall. Figure 12a shows the observed OLR pattern during DJF 1982–1983. (These data are not available before June 1974.) The simulated Pr83an distribution (Figure 11b) is consistent with observed OLR over South Africa and the adjacent Indian Ocean. Zimbabwe is about midway between the lowest OLR to the north, signifying the highest convective towers, and OLR maxima to the southeast and southwest, representing a dearth of convective activity. Contrast this with the OLR pattern during the very rainy DJF 1980–1981 (Figure 12b) when the axis of the highest clouds passed over the northern part of the country. Figure 12a also shows that more convective activity occurred over the southwestern Indian Ocean during DJF 1982–1983 than two years earlier, which is also consistent with Pr83an.

6.2. NORDESTE (4–12° S, 37.5–47.5° W)

6.2.1. *Background*

Within the region designated Nordeste, some precipitation is recorded during every month of the year, but the largest totals occur during March–May. The large

Figure 10 (facing page). November–March average precipitation rates (mm day^{-1}) for ensemble of five GCM simulations: (a) 1972–1973; (b) 1982–1983; (c) 1973–1974.

Figure 11 (facing page). November–March average precipitation rate anomalies (mm day^{-1}) relative to model 1970–1991 means for ensemble of five GCM simulations: (a) 1972–1973; (b) 1982–1983; (c) 1973–1974.

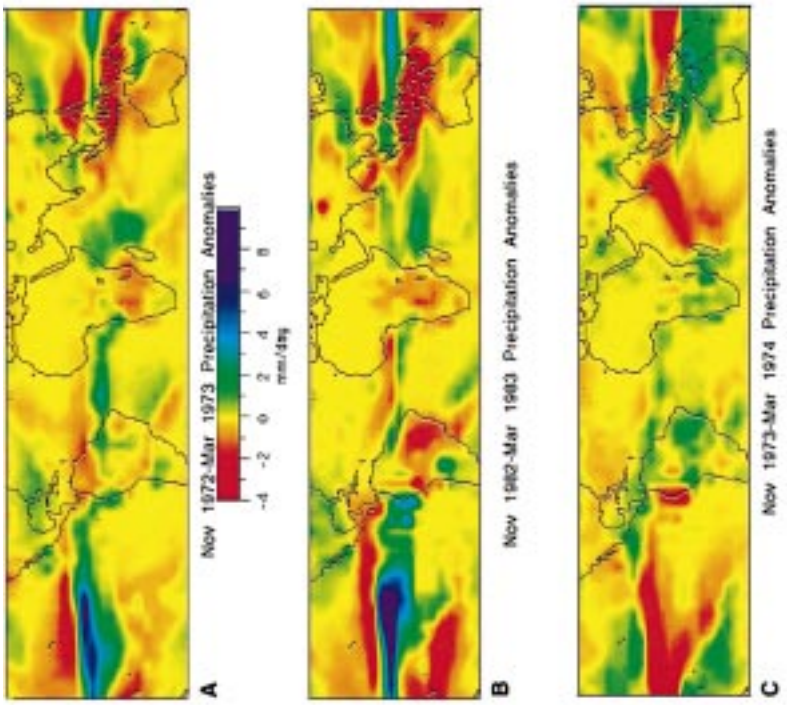

Figure 11

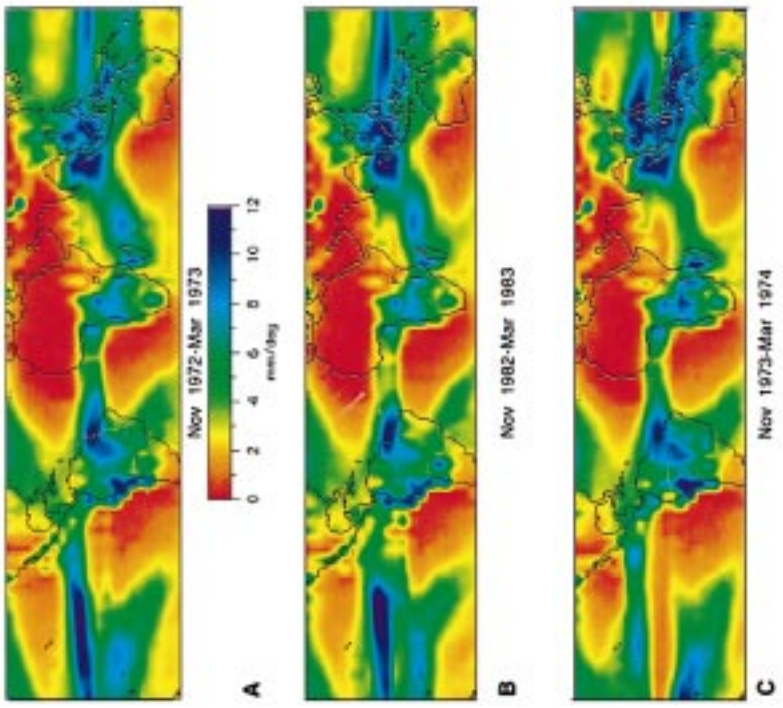

Figure 10

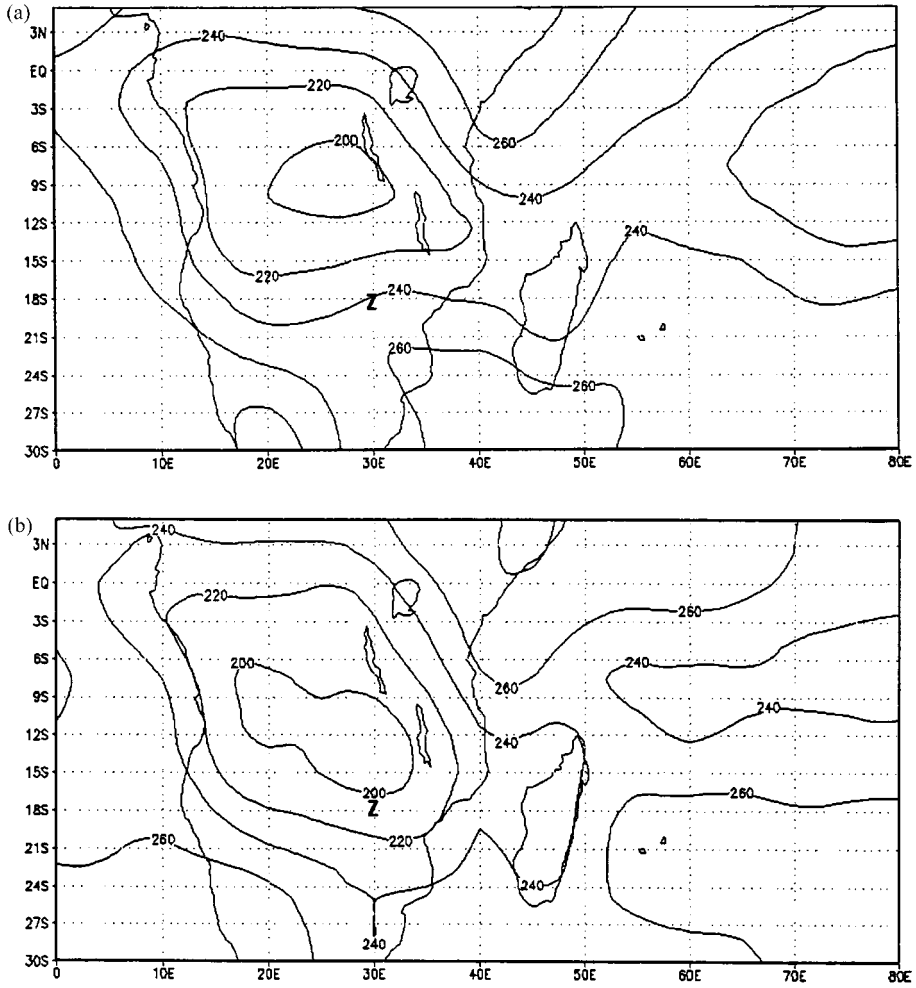

Figure 12. Satellite observed Outgoing Longwave Radiation (W m^{-2}). (a) December 1982–February 1983; (b) December 1980–February 1981. (Courtesy of Climate Diagnostics Center, http://www.cdc.noaa.gov/). **Z** marks the location of Zimbabwe.

interannual variability of rainfall there has been marked by occasional droughts, and resulting famines have prompted large migrations of population (Chu, 1991). Nordeste experiences a smaller annual rainfall than the rest of Brazil, less than 800 mm over most of the area and less than 500 mm over certain interior portions (Kousky and Chu, 1978). Over northern Nordeste, the sharp March–April peak in rainfall corresponds to the southernmost excursion of the Inter-Tropical Convergence Zone (ITCZ) to about 5° S.

Research has determined correlations between Nordeste precipitation and the ENSO indexes, but SST anomaly patterns in the tropical Atlantic Ocean have been shown to be even more strongly correlated with Nordeste rainfall accumulations. In

this regard, the influences of SST anomalies are well understood and are discussed below.

Ropelewski and Halpert (1987) found that sixteen out of seventeen warm ENSO phase episodes from 1911–1983 coincided with below normal rainfall over north-eastern South America (north equatorial Brazil, French Guiana, Surinam, Guyana and Venezuela). Nine of eleven extreme droughts (lowest 30% of ordered seasonal precipitation totals), but none of the very rainy seasons during this period, also correspond to El Niño occurrences. Chu (1991) attributes these dry spells to large-scale circulation mechanisms associated with El Niño: the sinking branch of the Pacific Walker cell may be relocated over South America to accommodate the eastward displacement of the rising branch to the mid-Pacific. During a (warm) El Niño, anomalously strong convection along the Pacific coast of South America is thought to promote subsidence over the interior of the continent, increasing the probability of drought for Nordeste. Conversely, the subsidence of La Niña along the Pacific coast encourages compensating convection that enhances Nordeste rainfall. For example, the Nordeste drought during the 1983 warm phase of an ENSO cycle contrasted sharply with rainier conditions that occurred during the following year when the Southern Oscillation Index had become positive.

A composite of the 10 driest years during 1912–1972 in Nordeste features positive March–April sea surface temperature anomalies (SSTA) in the northern tropical Atlantic and negative SSTA south of the equator (Hastenrath and Heller, 1977). Since the ITCZ tends to follow the latitude of highest SST, positive SSTA in the tropical North Atlantic favor an abbreviated southward migration of the ITCZ, which may even remain north of the Equator (Mechoso et al., 1990). During such drought seasons, near-surface northeasterly circulation from the North Atlantic is weakened and the main areas of moist convection remain north of Nordeste. Wet years have approximately the reverse pattern: cool SST occur to the north and warm SST to the south, favoring stronger anticyclonic circulation north of the Equator and deeper penetration of ITCZ-related moist convection into the Southern Hemisphere.

Interhemispheric SST gradients exert a hydrostatic influence on the lower tropospheric thickness pattern, modulating the north-south surface pressure gradient and consequently the near-surface meridional winds. Since the axis of maximum SST in the Atlantic is north of the equator, warm SSTA there, associated with dry seasons in Nordeste, enhance the pressure gradient south of the Equator, driving stronger southeasterly trade winds while weakening the northeasterly trades (Hastenrath and Druyan, 1993; Hastenrath and Greischar, 1993a). Correlations between monthly Nordeste precipitation and Atlantic SST are strongest in April and May, with positive correlations relative to the North Atlantic and negative correlations relative to the South Atlantic (Uvo et al., 1998).

Hastenrath and Greischar (1993b) found pre-season rainfall accumulations (presumably via ground moisture), meridional winds and SST over the Atlantic to be important statistical predictors of May–June Nordeste precipitation. Adding

a tropical Pacific SST index improved prediction skill, but it was a poor predictor by itself. Ward and Folland (1991) reported the predictability of 55% of the February–May Nordeste rainfall variance using only global distributions of SST predictors. All of these predictors are explicitly computed in the GCM and presumably influence the simulated Nordeste precipitation rates.

Moura and Shukla (1981) demonstrated with a simple analytical model that Nordeste droughts are associated with subsidence as part of a meridional circulation prompted by the colder tropical South Atlantic SST adjacent to Nordeste, in juxtaposition to convergence over the warmer SST to its north. Case studies of subsequent years (Marengo and Hastenrath, 1993) have sustained these findings. Mechoso and Lyons (1988) obtained realistic 1984 minus 1983 positive differences in Nordeste rainfall with GCM simulations forced by observed SST. Mechoso et al. (1990) further showed that the warm SSTA of the tropical South Atlantic in the late (austral) summer of 1984 were associated with increased convection over Nordeste despite weakened southeast trades and therefore sluggish westward moisture flux from the South Atlantic.

Experiments with the $8 \times 10^{\circ}$ resolution GISS Model II (Hastenrath and Druyan, 1993) forced with globally observed SST showed the aforementioned relationship between SST gradients and atmospheric pressure gradients. However, that model's poor tropical circulation and unrealistic precipitation climatology, in part a consequence of the coarse horizontal resolution, produced 1980–1986 interannual variations of March–April Nordeste rainfall that were poorly correlated with observations.

We created a time series of monthly precipitation anomalies based on NOAA/NCDC archived station observations within the rectangular area bounded by 4–12° S, 37–48° W. For the period 1969–1991, the correlation between 5-month running means of these Nordeste precipitation anomalies and

(1) 5-month running means of SOI anomalies is 0.25,
(2) 5-month running means of Niño3 SST anomalies (N3A) is –0.31,
(3) 5-month running means of an Atlantic Ocean SST anomaly index (AOI) is 0.47,

where the AOI is the south minus north difference in SST anomalies between the areas 0°–24° S, 10–40° W and 0°–24° N, 20–50° W. Together in a multiple regression, the AOI and N3A account for 27% of the variance of the observed record ($R = 0.52$). The SOI anomaly does not significantly add to the explained variance when N3A is included.

6.2.2. *GCM Simulations – Precipitation*

Our analysis of model results refers to monthly mean precipitation anomalies. The time series of simulated Nordeste precipitation anomalies are a reasonable representation of observations during several intervals of the 1969–1991 simulations (Figure 13a). The correlation between the ensemble mean simulation and obser-

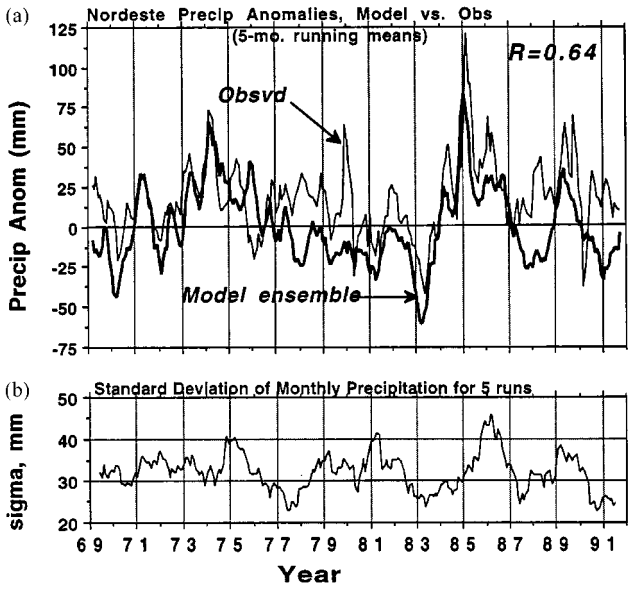

Figure 13. (a) Five-month running means of precipitation rate anomalies (mm) for Nordeste. 'Model' refers to ensemble values that are departures from 23-year monthly means, averaged over the area 4–12° S, 37.5–47.5° W. Observations are departures from the base period 1951–1980, based on precipitation measurements averaged over the same area and archived at NCDC (Courtesy of http://www.ncdc.noaa.gov/onlinedata/climatedata/). (b) Eleven-month running means of the standard deviation (mm day^{-1}) between the modeled precipitation rates of the five simulations over the same area (above).

vations increases steadily with increased smoothing of both time series. Thus, the optimal time scale for realistic simulations of SST-forced Nordeste precipitation anomalies is seasonal rather than monthly. Without smoothing, the correlation coefficient is only 0.35, increasing to 0.55 (which is significant at the 99% level) for 3-month running means and to 0.64 (also significant at the 99% level) for 5-month running means. This last correlation is slightly higher (0.75) against observed anomalies from station data (usually 26–27 stations) supplied by Hastenrath and Greischar, but the main features of the model validation remain the same. Are these results likely to be less significant if they had been based on more than five simulations? We examined modeled Nordeste precipitation from an archived ensemble of ten simulations of another version of the GISS GCM to estimate the correlations' sensitivity to ensemble size. We found that the correlation coefficients of 3-month and 5-month running means were 0.06 higher for the 10-run ensemble than for a sub-set of five runs, so it is likely that results from the 5-run ensemble used in our study do not overestimate statistical significance.

Figure 13b shows the smoothed time series of the standard deviation (σ) of modeled Nordeste precipitation anomalies between the five individual runs. Lower σ indicate a greater consensus among the five runs regarding the values of sim-

TABLE I

Correlation coefficients between model ensemble mean Nordeste precipitation anomalies (relative to model's 1969–1991 base period) and three indexes monitoring forcing influences. All time series are represented by 5-month running means. N3A refers to the Niño3 SST anomaly index and AOI is the Atlantic Ocean SST anomaly index defined in the text. All correlation coefficients are significant with greater than 99% statistical confidence

N3A	SOI anomaly	AOI	Multiple (N3A and AOI)
–0.48	0.48	0.71	0.79

ulated anomalies. According to Figure 13a, observed positive or negative rainfall anomalies were reproduced by the ensemble mean for many seasons. However, for some of those years, a relatively high σ suggests that the SST forcing was not very decisive. On the other hand, a high degree of consensus *was* achieved for several of the realistic hindcasts: negative departures during 1970 and 1983; positive anomalies during 1974, 1977, 1984 and 1985. We note especially that the skillful simulation of the 1983 drought involved strong SST forcing related to an El Niño event. Curiously, the rather large observed positive anomalies of 1980, 1988 and 1991 were missed by a consensus of the simulations. Between January 1983 and January 1987 the correlation between model ensemble means and observations shown in Figure 13a was especially high ($R = 0.86$). This period includes the drought of 1983 and excess rains during 1984 and 1985. A moderately pronounced El Niño in 1987 apparently forced the Nordeste climate into yet another simulated drought. Our observational data indicate that the observed anomalies during 1987 were near zero, but they nevertheless constituted a *relative* minimum. Also, positive anomalies observed (but not simulated) during the peak of the 1988 rainy season are consistent with the occurrence that year of strong La Niña conditions.

The simulated Nordeste precipitation anomalies were even better correlated with the SOI and SST indexes than our observed precipitation data (Table I). One explanation is that our SST data is too approximate of actual ocean conditions. Thus the correlation between observed Nordeste precipitation anomalies and a more representative SST analysis could be higher. Alternatively, these results could imply that the GCM is more sensitive to the SST forcing than the real world.

The hypothesis that strong SST forcing encourages consensus among the simulations of Nordeste precipitation anomalies was examined. Table II shows the correlations between σ and each of three forcing indexes as well as the multiple correlation coefficient related to all three indexes. Absolute values of the indexes were used since strong forcing is implied by large positive or negative anomalies.

The standard deviation of monthly precipitation anomalies between the five simulations (σ) shows a strong annual cycle. By taking 11-month running means,

TABLE II

Correlation coefficients between (11-month running means of) the standard deviation of Nordeste precipitation anomalies (relative to model's 1969–1991 base period) for five simulations and absolute values of three indexes monitoring forcing influences. The time series of the indexes are represented by 5-month running means. All correlation coefficients are significant with greater than 99% statistical confidence

Absolute values of:			
Niño3 SSTA	SOI anomaly	AOI (see text)	Multiple, all three
–0.30	–0.25	0.33	0.43

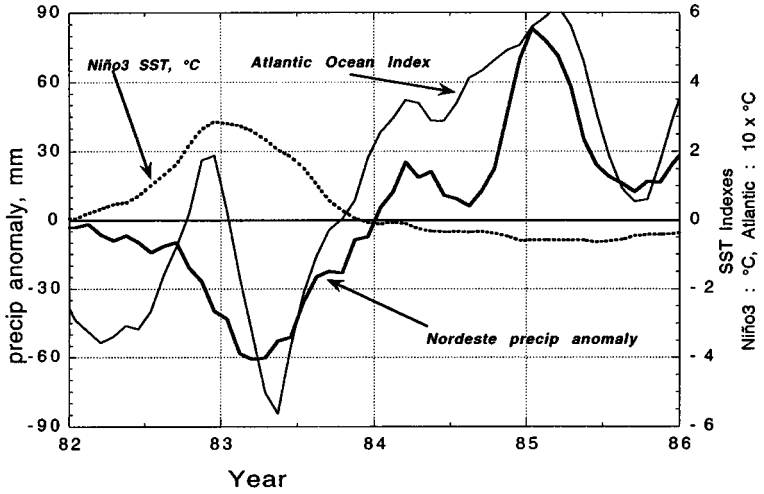

Figure 14. Time variation of Niño3 SST anomalies, Atlantic Ocean Index and model ensemble Nordeste precipitation anomalies, shown as 5-month running means between 1982–1986.

the annual cycle is filtered. The 11-month running means of σ were plotted against 5-month running means of Niño3 SST anomalies (N3A). The threshold of $\sigma = 36$ mm seems to be associated with N3A of ± 1°C such that strong SST forcing ($|\text{N3A}| > 1$ °C) always resulted in low σ (<36 mm). On the other hand, weak N3A forcing produced a range of results, sometimes a high degree of consensus, sometimes not. Given the dependence of Nordeste precipitation on SST anomaly gradients in the Tropical Atlantic (see above) it seems reasonable that σ (for the Nordeste precipitation simulations) should also be influenced by SST forcing in the Tropical Atlantic Ocean. However, we found a positive correlation ($R = 0.33$) between the absolute value of AOI and σ. There were many months for which σ was relatively high despite the strong SST anomaly gradient represented by AOI. Some of this behavior can be explained by the association of enhanced rain events with high AOI, since σ tends to be larger for months with heavier precipitation.

6.2.3. *Analysis of Selected Seasons*

SST anomalies in the Eastern Equatorial Pacific, represented by N3A, peaked in December 1982, followed by a cooling to negative values during 1984–1985 (Figure 14). This negative SST trend coincided with the rebound of model ensemble mean precipitation over Nordeste, from large deficits in 1983 to anomalously rainy conditions during early 1985. We have previously shown that this simulated precipitation trend was quite faithful to the observational record (Figure 13). In addition, Figure 14 shows that the precipitation anomaly minimum in 1983, the subsequent increases thereafter and the eventual peak in 1985, were closely mirrored by variations of the AOI. Experimental simulations will be required to determine the relative influences of the two oceans on this trend in rainfall anomalies over Nordeste.

The upper tropospheric circulation during Nordeste's peak MAM rainfall season features a broad center of divergence over the Maritime Continent and centers of convergence above the subtropical anticyclones over the southeastern Pacific and the South Atlantic. The center of upper tropospheric divergence corresponds to a minimum in 200 mb velocity potential (χ_2) and the foci of convergence correspond to maxima in χ_2 (Figure 15a). The moist convection characterizing South American precipitation during MAM form a col of minimum χ_2 over the continent. Enhanced convection over positive SST anomalies in the southeast Pacific during MAM 1983 weakened the strength of the upper tropospheric convergence considerably, lowering the χ_2 maximum relative to the long term mean (Figure 15b). The strength of upper tropospheric convergence over the anticyclonic regimes was particularly eroded along 6–10° N over the eastern Pacific Ocean and over the North Atlantic, as evidenced by negative χ_2 anomalies that extend eastward from the Pacific, across northern South America to the North Atlantic Ocean (Figure 15c). This pattern of modeled χ_2 anomalies is quite realistic, judging by comparison to the corresponding NCEP reanalysis (Figure 15d), although negative departures over the Equatorial East Pacific are less extreme for the GCM. The northern coast of South America near the Guyanas and the mouth of the Amazon, affected by this region of enhanced moist convection, has been identified as one node of a convective dipole whose other node over Northeast Brazil experiences negatively correlated vertical motion anomalies (Mechoso et al., 1990; Marengo et al., 1993). Nordeste drought, as in MAM83, is often associated with a weakened North Atlantic anticyclone and an ITCZ that stalls to the north of Nordeste. Thus, enhanced moist convection during MAM83 across the northern coast of South America, apparently related to El Niño warming of the adjacent Pacific, reduced convection to the south resulting in deficient MAM rainfall in Nordeste.

The simulated χ_2 anomaly distribution corresponding with the very rainy period in MAM 1985 indicates a stronger than usual divergent upper tropospheric planetary circulation. This is characterized by stronger than normal χ_2 maxima over the Eastern Pacific/northern South America combined with negative anomalies over Indian Ocean areas of convection (Figure 16a). The positive χ_2 anomaly implying

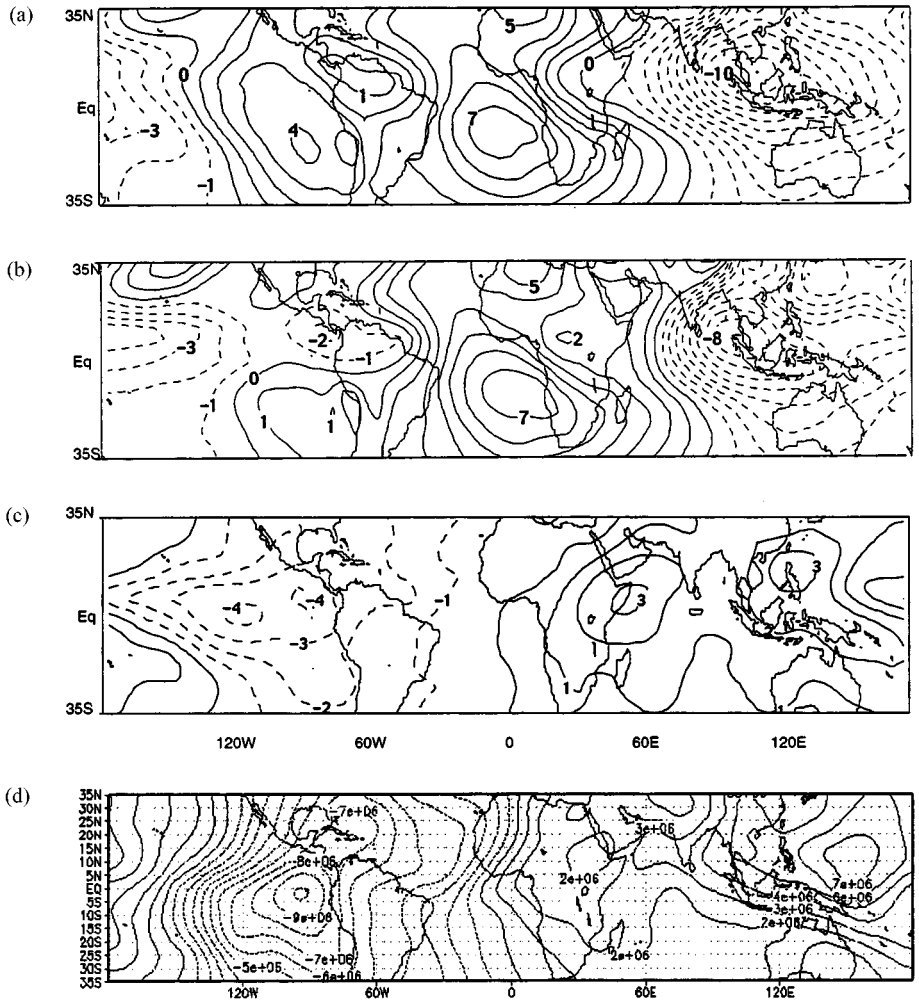

Figure 15. Velocity potential of the level 7 (200 mb) circulation for March–May. (a) Model ensemble mean, 1969–1991; (b) Model ensemble mean, 1983; (c) Modeled 1983 anomalies, (b) minus (a); (d) NCEP reanalysis 1983 anomalies (relative to base period, 1979–1995). (Courtesy of Climate Diagnostics Center, www.cdc.noaa.gov/ncep_reanalysis.) Units: 10^6 m^2 s^{-1}.

strong upper tropospheric convergence and subsidence along 10° N over the Eastern Pacific is a consequence of co-located anomalously cold SST during this season and is consistent with inhibited moist convection over Colombia and Venezuela. Immediately to the southeast, vigorous moist convection which generated abundant rainfall in Nordeste during MAM 1985 is in part a response to the subsidence that is implied by this χ_2 maximum, as discussed above. The NCEP analysis of χ_2 anomalies for MAM 1985 (Figure 16b) suggests several discrepancies in the modeled results, but it validates the positive χ_2 anomalies over northern South America as

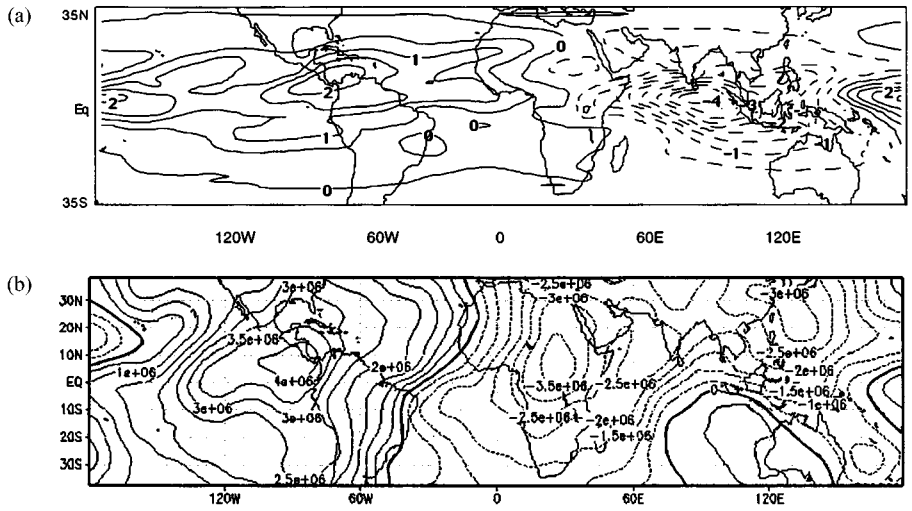

Figure 16. Velocity potential anomalies of the level 7 (200 mb) circulation for March–May 1985. (a) Model ensemble mean, relative to 1969–1991; (b) NCEP reanalysis anomalies (relative to base period, 1979–1995). (Courtesy of Climate Diagnostics Center, www.cdc.noaa.gov/ncep_reanalysis.) Units: 10^6 m^2 s^{-1}.

well as the increased polarity of the χ_2 field between the Western Hemisphere and the Indian Ocean.

The rather coarse 4° meridional resolution of the model grid can marginally resolve typical interannual shifts in the latitude of the ITCZ confluence near Nordeste. Our analyses of April 1983 circulation detect a displacement of the ITCZ that is consistent with the model's simulation of precipitation deficits over Nordeste. Figure 17a shows the model ensemble mean circulation at level 1 (985 mb) for April 1983, the month of the southernmost excursion of the ITCZ over Northeast Brazil. Confluence between the northeasterlies of the North Atlantic and the southeasterlies of the South Atlantic intersects the Brazil coast quite close to the Equator. The April 1983 resultant wind over Nordeste is easterly and southeasterly, a further indication that the ITCZ has stalled to the north. Contrast this with corresponding April resultant winds for the entire 22-year simulation (Figure 17b) with a confluence/ITCZ position closer to 5° S. In this model climatology, the April circulation over northern Nordeste (2° S) is northeasterly, implying an ITCZ position bisecting this region.

The northward displacement of the ITCZ simulated for April 1983 is seen more clearly by examining the anomaly of the meridional component (v) of the lower tropospheric circulation. Figure 18a shows that the v anomalies at the model's lowest layer were positive over Nordeste and over the Equatorial Atlantic, indicating a stronger April 1983 southerly component of the southeast Trades. This pattern is validated by the NCEP reanalysis of the v anomalies at 925 mb (Figure 18b) which shows even stronger southerly anomalies. In both analyses, positive anomalies

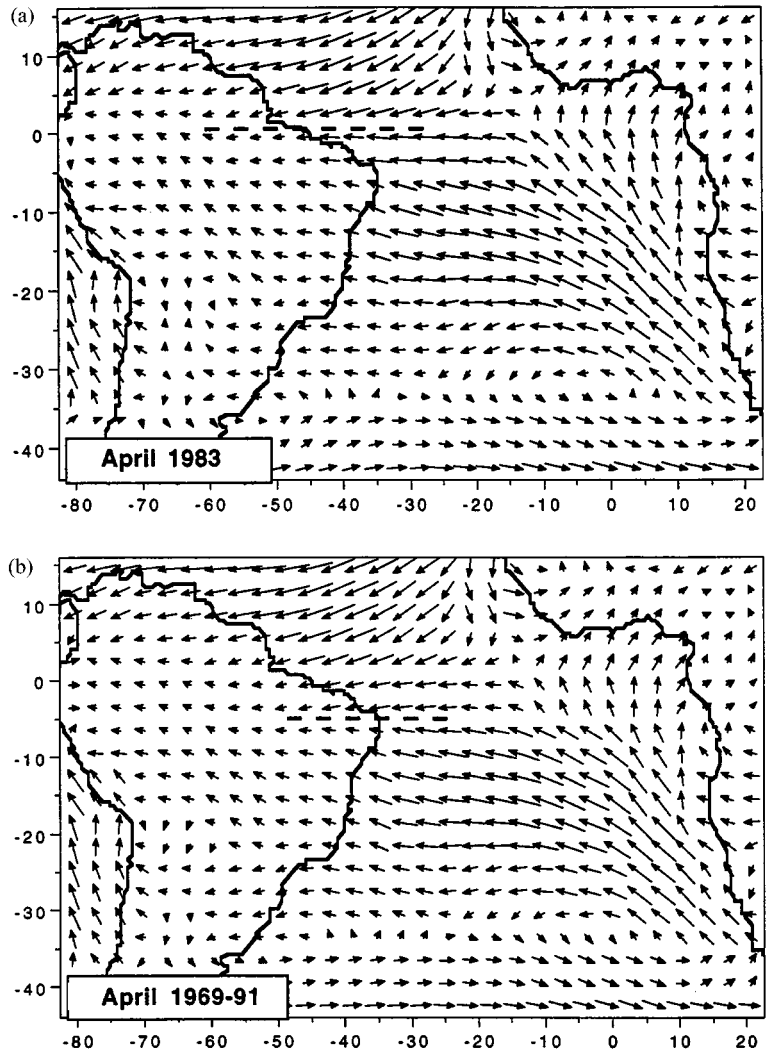

Figure 17. (a) Model ensemble circulation for April 1983 at level 1 (985 mb). (b) Model ensemble circulation for April 1969–1991 at level 1 (985 mb).

north of the Equator represent the weakened northerly component of the northeast Trades during April 1983.

The implied position of the ITCZ in the April 1985 simulated 985 mb circulation over northeast Brazil bisects Nordeste near 5° S (Figure 19a), clearly south of the confluence simulated for the much drier April 1983 (Figure 17a). Negative v anomalies (Figures 19b,c) along and north of the Equator indicate that the simulated and observed Northeasterly Trades were stronger than normal while southeasterlies south of the Equator were weaker than their long-term means. These circula-

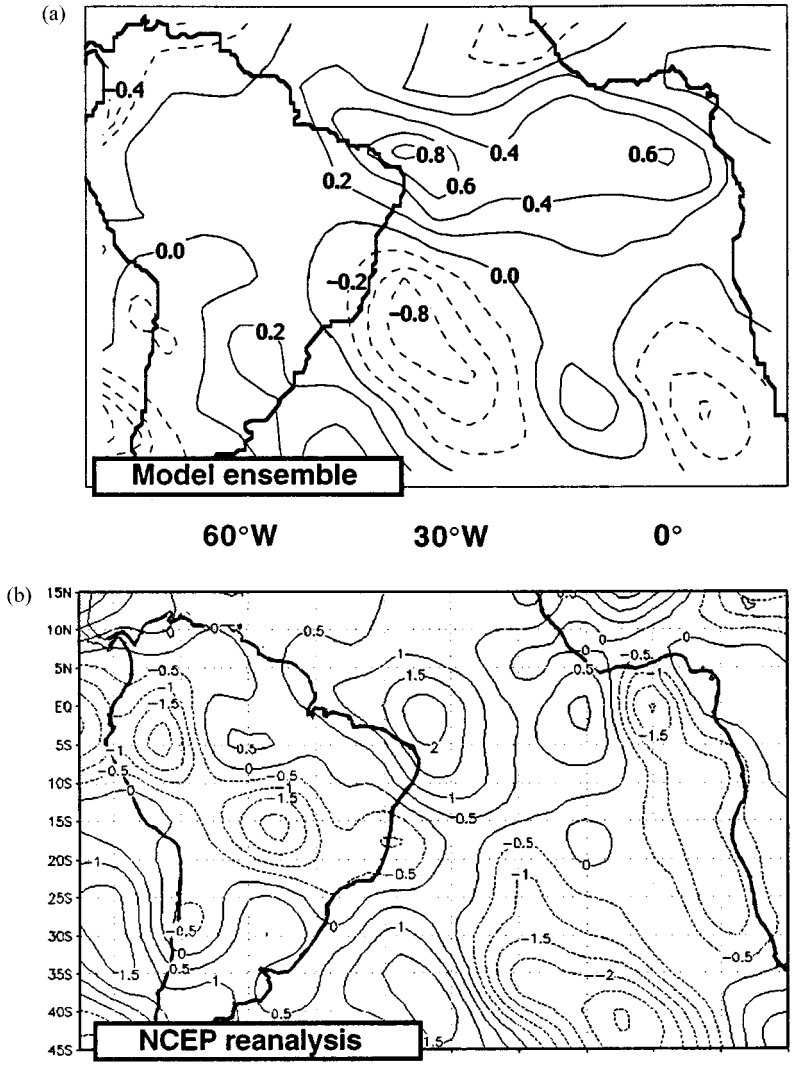

Figure 18. (a) Meridional component of April 1983 resultant wind for model ensemble at level 1 (985 mb). (b) Meridional component of April 1983 resultant wind for NCEP reanalysis at 925 mb. (Courtesy of Climate Diagnostics Center, www.cdc.noaa.gov/ncep_reanalysis.) Units: m s^{-1}.

tion characteristics have been associated with surplus precipitation in Nordeste in several studies (Hastenrath and Druyan, 1993; Hastenrath and Greischar, 1993a).

The influence of ITCZ meridional displacements on Nordeste rainfall anomalies is apparent in the examples of April 1983 and April 1985, shown in Figures 20a,b. Deficits occur along 5–10° S during April 1983, from Nordeste to the South Atlantic in juxtaposition to enhanced precipitation within the more northerly parallel zone centered along 0–5° N. Observations available from NOAA/NCDC (not shown) confirm the widespread negative anomalies over Northeast Brazil as well as

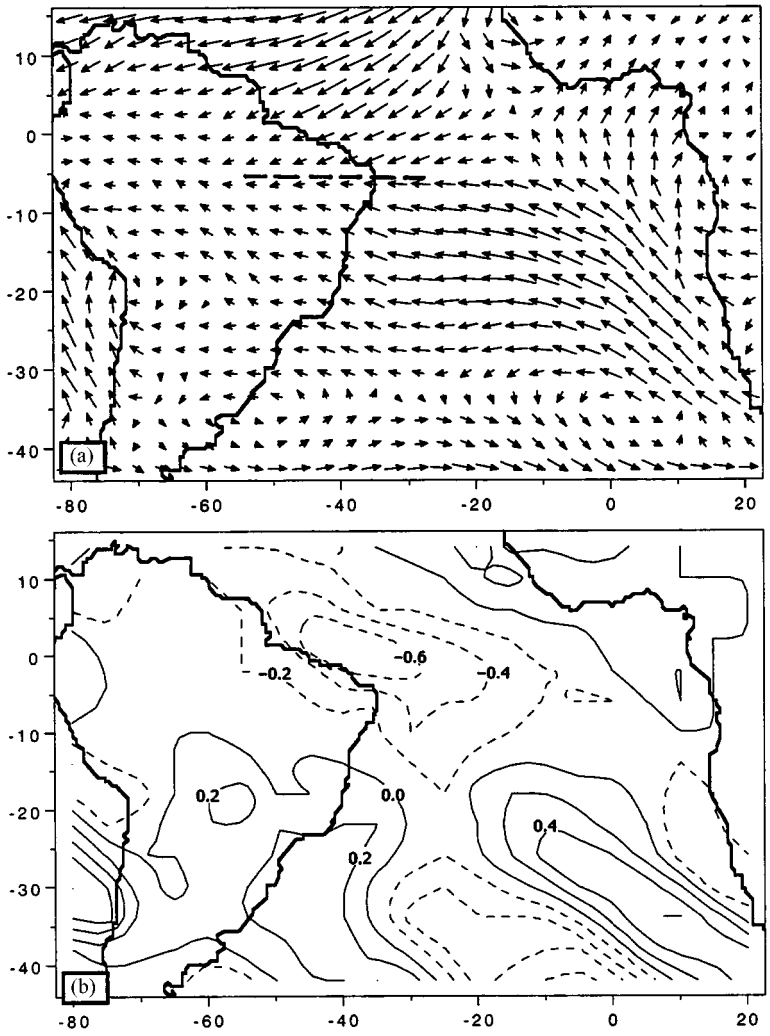

Figure 19a,b.

the area of positive anomalies simulated for southern Brazil and Paraguay. Direct observations of precipitation were not available for the Atlantic coastal waters, but the NCEP reanalysis precipitation anomaly fields for April 1983 and 1985 (Figures 20c,d) confirm the simulated dipole patterns between 2° N and 10° S over Brazil, as well as the positive anomalies over southern Brazil during April 1983.

These findings echo conclusions of previous studies, most notably Mechoso et al. (1990), who relate this Nordeste drought to positive SST anomalies in the North Atlantic Ocean during March–April 1983. We plan additional GCM simulations to investigate the relative importance of Pacific and Atlantic SST anomalies to Nordeste rainfall deficits.

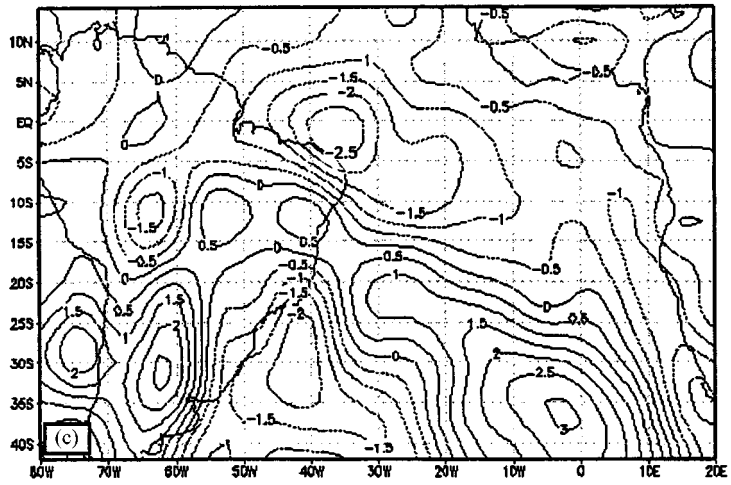

Figure 19c.

Figure 19. (a) Model ensemble circulation for April 1985 at level 1 (985 mb). (b) Meridional component of April 1985 resultant wind for model ensemble at level 1 (985 mb). (c) Meridional component of April 1985 resultant wind for NCEP reanalysis at 925 mb. (Courtesy of Climate Diagnostics Center, www.cdc.noaa.gov/ncep_reanalysis.) Units: m s^{-1}.

6.3. U.S. CORN BELT (36–44° N, 87.5–97.5° W)

Rainfall in this region is recorded during each month of the year. However, U.S. Corn Belt precipitation usually peaks during May–August which experience monthly means of near 100 mm or about double those of January–February. The seasonal cycle in the simulations is slightly out of phase in that the modeled maximum rainfall of about 115 mm $month^{-1}$ occurs in March–May and the minimum in September–October. Because of this region's extratropical latitude, we expect most of the interannual climate variability to be chaotic and not explained by SST anomaly variations (Hansen et al., 1997). However, extremes in the ENSO cycle may 'load the dice' in favor of droughts or floods. Our model ensemble 5-month running means of precipitation over the U.S. Corn Belt were significantly correlated with Niño3 SST ($R = 0.52$). Handler (1986) found that El Niño years have been related with positive maize yield anomalies in the U.S. Corn Belt and La Niña with negative maize yield anomalies based on data from 1868–1982.

Five-month running mean precipitation anomalies, model versus observations, were compared. Overall, the correlation between the model ensemble-mean anomalies and the observed rainfall anomalies is small and insignificant. This was also the case for an ensemble of ten simulations with another model version. Given the overall lack of correlation between simulated and observed precipitation anomalies for the U.S. Corn Belt, predictive skill cannot be attributed to the model for this region. However, there is some indication that the simulations provide more robust

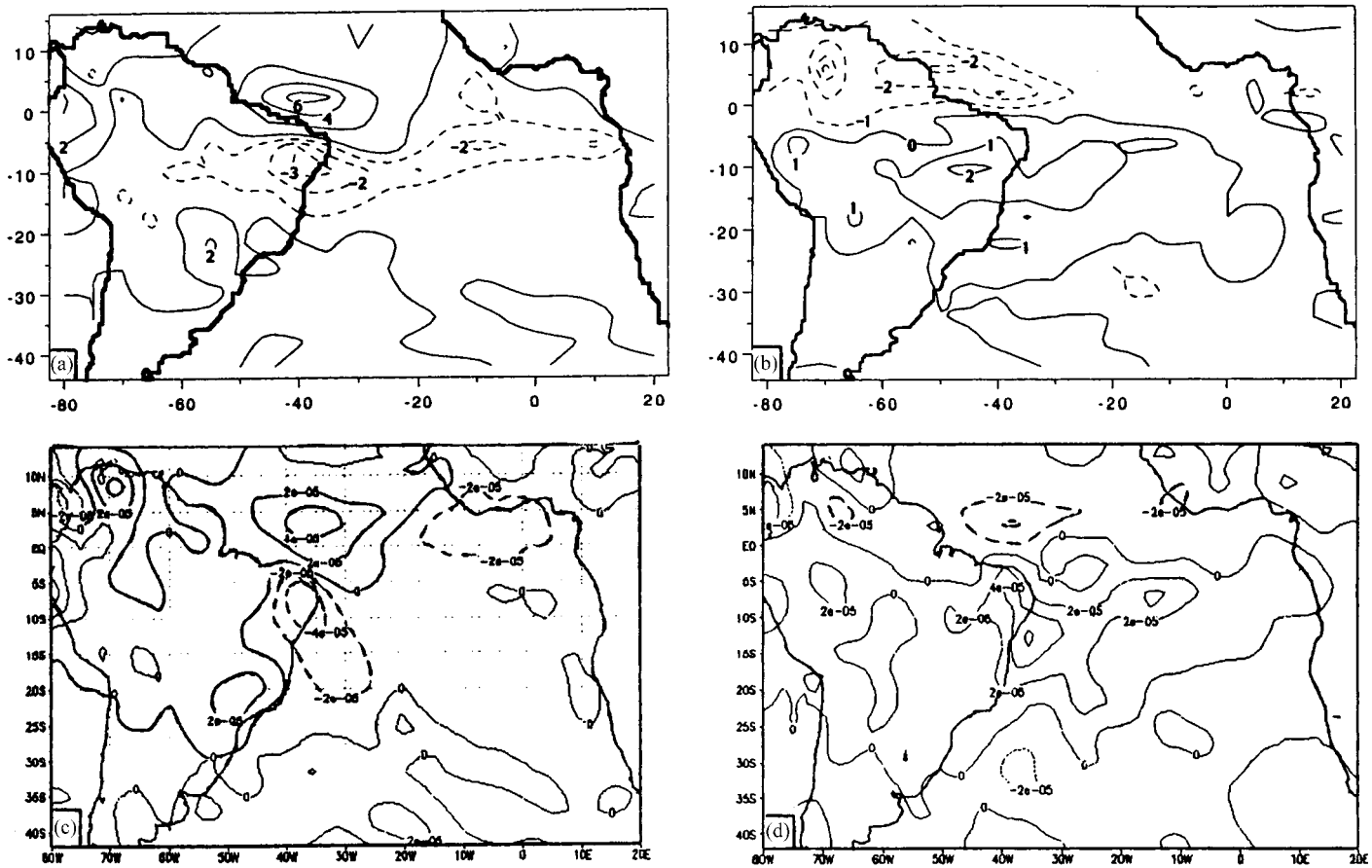

Figure 20. Precipitation anomalies. (a) Model ensemble simulation for April 1983, relative to 1969–1991; (b) Model ensemble simulation for April 1985, relative to 1969–1991; (c) NCEP reanalysis, April 1983, relative to 1979–1995; (d) NCEP reanalysis, April 1985, relative to 1979–1995. ((c) and (d) courtesy of Climate Diagnostics Center, www.cdc.noaa.gov/ncep_reanalysis.) Units for GCM: mm day^{-1}. Units for NCEP: 10^{-5} kg m^{-2} s^{-1} = 0.86 mm day^{-1}.

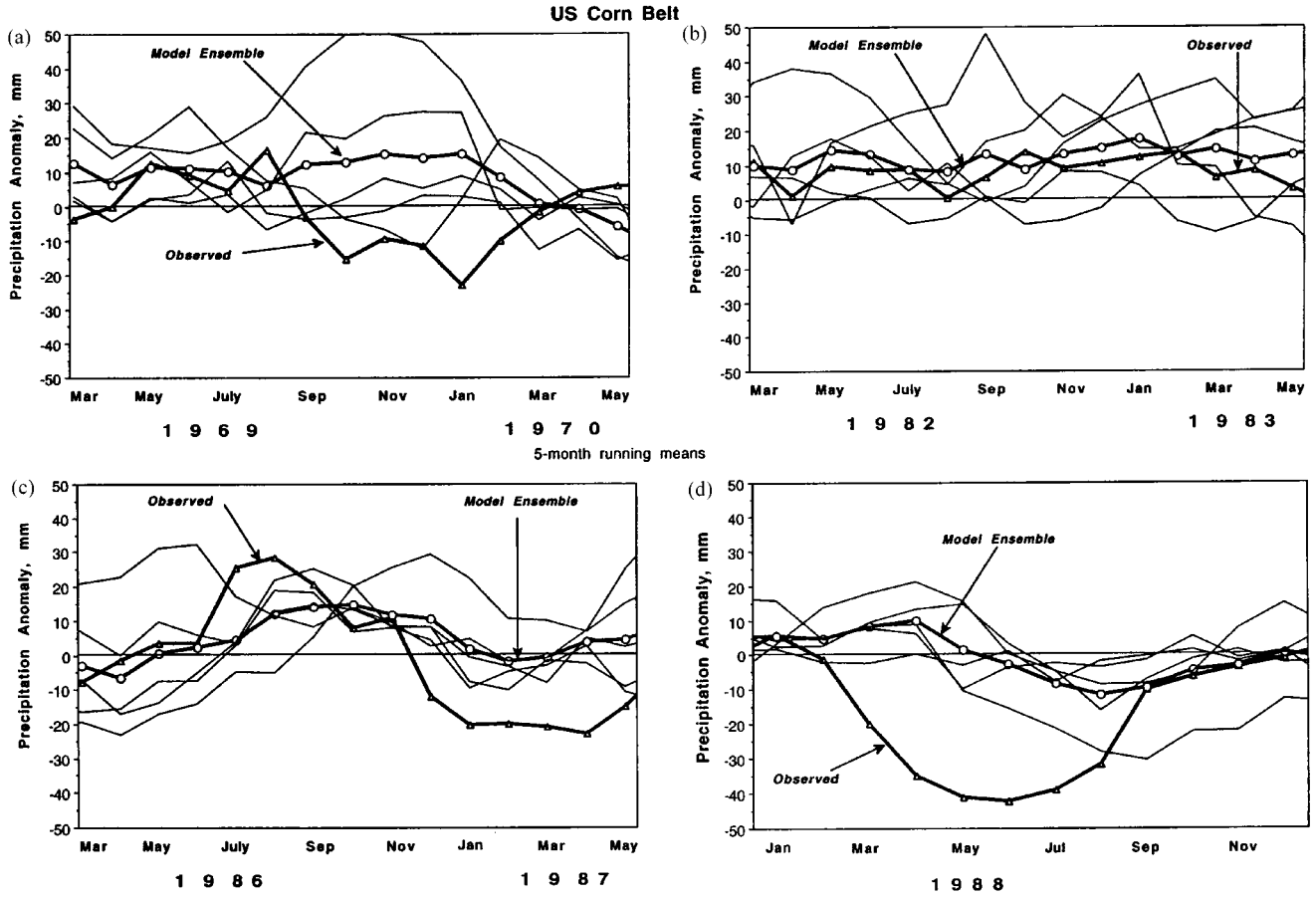

Figure 21. Time series segments of 5-month running mean U.S. Corn Belt region precipitation anomalies (mm) for five simulations, their ensemble mean and corresponding observations. (a) March 1969–May 1970; (b) March 1982–May 1983; (c) March 1986–May 1987; (d) January 1988–December 1988.

results during extreme ENSO events as a consequence of the forcing from highly organized SST anomaly patterns. For example, all of the simulations indicate positive precipitation anomalies during the summer of 1969 (Figure 21a) (Niño3 SST > 0), and positive anomalies were indeed observed. Late in 1975, when Niño3 SST < 0, there is a near consensus for negative anomalies and this also corresponds to actual deficits. The ensemble mean correctly indicates positive anomalies during 1982 (Figure 21b) (Niño3 SST > 0), but the wide dispersion between the individual model simulations belies any consensus in this case. Most of the simulations did agree, however, on the anomalously rainy conditions that were in fact observed during the summer and fall of 1986 (Figure 21c). The consensus was particularly high for the months of September–November, a period of a building El Niño in the tropical Pacific.

The spring and summer of 1988 were especially dry in the U.S. Corn Belt, with large negative precipitation anomalies occurring each month, April–August. The smoothed time trend bottomed out at –42 mm in June (Figure 21d). Model ensemble 5-month running means of precipitation anomalies for the region (Figure 21d) were indeed negative spanning the months June–November, and July–August 1988 anomalies for the five simulations ranged from –3.0 mm to –24.9 mm. The ensemble mean July–August 1988 anomaly was small, at –10.0 mm, compared to the observed anomalies, and since this is only –1.1 standard deviations of July–August means over the 23 year simulation, it is not significantly different from the model climatology.

Additionally, we determined that a small dispersion between individual simulations of monthly precipitation rate for the U.S. Corn Belt did not consistently correspond to a lower range of model ensemble rainfall errors.

7. Discussion and Conclusions

We have analyzed the results of five simulations by the Model II' SI97 version of the GISS climate model, forced by globally observed monthly SST. The study has assessed how well model simulations with perfect SST information can predict seasonal rainfall anomalies in Zimbabwe, Brazil's Nordeste and the U.S. Corn Belt, three agricultural regions with high economic sensitivity to climate impacts. Precipitation accumulations in each of these regions has been shown by previous studies to be sensitive to the ENSO cycle. Although drought often occurs in Zimbabwe and Nordeste during El Niño years, other factors can mitigate the outcome. Many such influences are accounted for by climate models.

Simulated atmospheric first order responses to prescribed SST forcing in these simulations validate well with observational evidence over the Tropical Pacific Ocean. They give a clear expression of interannual variability closely associated with ENSO. Specifically, correlations of time series of modeled mid-tropospheric temperatures versus MSU observations range from 0.66–0.74, and the ensemble

mean of time-smoothed SOI anomalies is even better correlated with the corresponding time series of observations ($r = 0.86$). Concomitant with the realistic simulation of these ENSO cycles over the tropical Pacific, we showed that the ensemble mean of five simulations captured the waxing and waning of lower tropospheric westerly wind anomalies characteristic of El Niño episodes. Corresponding patterns of negative OLR anomalies indicate the sensitivity of the GCM's moist convection to the destablizing influence of anomalously warm in situ SST. There is, however, considerable variability between individual simulations and modeled extremum of climate variables are somewhat damped compared with observations.

Model ensemble precipitation rates for the November–March rainy season in Zimbabwe were not significantly correlated with the observational record over the 22-year length of the simulations. Even with perfect SST, the GCM is not a reliable tool to consistently predict Zimbabwe seasonal rainfall anomalies. However, there is evidence that the simulation of rainfall anomalies of the correct sign during selected seasons was not mere chance. Large precipitation deficits were correctly hindcast during two El Niño seasons with a rather high degree of consensus between the five model runs. We conclude that strong and well organized SST forcing was decisive in evolving circulation patterns that inhibited copious Zimbabwe precipitation during those years in most of the simulations. Since extreme precipitation anomalies have the greatest impact on climate sensitive agriculture, a similar result in a pure forecast mode could provide the means for beneficial advice to the Zimbabwe farming community.

Our analysis of spatial circulation patterns during these two El Niño seasons, in the simulations and observations alike, detected a weakening of the overall upper tropospheric planetary divergent circulation, with regional enhancements of moist convection over the eastern tropical Pacific and the South Indian Ocean. During seasons with below normal Zimbabwe rainfall, the most active ITCZ lies to the north and convection over the country is inhibited by large scale subsidence. Modeled deficits over Zimbabwe during November–March 1972–1973 and 1982–1983 resulted from realistic spatial displacements of more typical (climatological mean) patterns. Realistic simulation of the synoptic patterns which led to drought increases confidence that these GCM hindcasts are more realistic than fortuitous.

Time series of simulated five-month running means of Nordeste (Brazil) precipitation are well correlated with observations. Decreases in the correlation coefficient for less heavily smoothed series indicate that, in this region, the model's temporal resolution for realistic results is seasonal rather than monthly. Additional research will need to determine how the degradation of prediction skill with increased (time) resolution affects agricultural applications, but skillful seasonal predictions are nevertheless potentially beneficial. For example, given a reliable projection of the seasonal departure of local rainfall, statistical analysis could suggest the probability of agriculturally relevant intraseasonal distributions of the anomalies.

We showed that model simulated Nordeste precipitation was correlated with SST anomaly patterns in the same sense as actual rainfall accumulations. In fact, higher correlations for the simulated values imply that our SST data may not be an accurate enough representation of real conditions. Alternatively, the GCM may be more sensitive to SST forcing than the actual climate system.

The strength of the ENSO signal influenced the consensus between individual simulations of Nordeste rainfall; extreme Niño3 SST anomalies led to a smaller range of predictions. As with Zimbabwe, extreme ENSO events seem to offer the best opportunity for useful precipitation predictions by the GCM.

The example of realistically simulated Nordeste drought during the 1983 El Niño featured an abbreviated southward excursion of the ITCZ, which kept the heaviest seasonal rainfall north of the region. We showed that the SST forced ensemble of simulations recreated the actual northerly displacement of the April 1983 confluence of southeasterly and northeasterly Trade Winds in conjunction with the corresponding northerly displacement of heavy ITCZ precipitation. On the other hand, rainier conditions for Nordeste during 1985 were correctly reproduced by the model's more southerly displacement of the ITCZ confluence and rainfall maximum, bringing it over the Nordeste region by April.

These SST forced simulations did not demonstrate the GCM's potential for a consistently useful prediction of seasonal rainfall anomalies in the U.S. Corn Belt. Empirical studies offer some indication that positive Niño3 SST is often related to positive rainfall anomalies in this region. We found support for this relationship in that the simulations gave a credible hindcast for a building El Niño during the fall of 1986, with all five runs indicating rainfall rates some 25–50% above the 23-year model means for those months. Similarly, dry conditions were simulated by all five runs during the summer of 1988 corresponding to an actual drought, but the simulated negative rainfall anomalies were a small fraction of the observed departures and not statistically significant.

Future modeling experiments will focus on the sensitivity of Zimbabwe, Nordeste and U.S. Corn Belt rainfall anomalies to controlled degradations of SST boundary data as an alternative to the 'perfect SST' approach used in this study. For example, we will test the consequences of persisting SST anomalies in one or more basins for up to three months. In addition, the relative contributions of specified SST in each major ocean to the interannual variability of regional precipitation will be determined in a carefully designed series of GCM simulations. Finally, additional simulations will compare changes in model physics and resolution to the results from these experiments.

Acknowledgements

This research was sponsored by NASA Earth System Science under Grant No. NCC5-117. We gratefully acknowledge support from the NASA Climate and Earth

Observing System Programs. We thank Jeffrey Jonas and Lilly Del Valle for their assistance in preparing Figures 3 and 4. LD received support from NSF Grant ATM-97-25142 and KS from NSF Grant ATM-96-28843.

References

Boer, G., Arpe, K., Blackburn, M., Déqué, M., Gates, W., Hart, T., Le Treut, H., Roeckner, E., Sheinin, D., Simmonds, I., Smith, R., Tokioka, T., Wetherald, R., and Williamson, D.: 1992, 'Some Results from an Intercomparison of the Climates Simulated by 14 General Circulation Models', *JGR* **97**, 12771–12786.

Boyle, J. S.: 1998, 'Evaluation of the Annual Cycle of Precipitation over the United States in GCMs: AMIP Simulations', *J. Climate* **11**, 1041–1055.

Chelliah, M., Ropelewski, C., and Rasmusson, E.: 1998, 'Low Frequency Variability and Composite Atmospheric Circulation over the Globe Associated with 'ENSO' Based on 40 Years of NCEP/NCAR Reanalysis Data', in Prepint Volume, *Ninth Conference on Global Change Studies*, AMS, Phoenix, AZ, pp. 192–195.

Chu, P-S.: 1991, 'Brazil's Climate Anomalies and ENSO', Chapter 3 in Glantz, M., Katz, R., and Nicholls, N. (eds.), *Teleconnections Linking Worldwide Climate Anomalies*, Cambridge University Press, New York, p. 43.

Del Genio, A. and Yao, M.-S.: 1993, 'Efficient Cumulus Parameterization for Long-Term Climate Studies. The GISS Scheme', in Emanuel, K. and Raymond, D. (eds.), *Cumulus Parameterization*, Amer. Meteorol. Soc. Monograph Series, Vol. 24, Boston, MA, pp. 181–184.

Del Genio, A., Yao, M.-S., Kovari, W., and Lo, K.-W.: 1996, 'A Prognostic Cloud Water Parameterization for Global Climate Models', *J. Climate* **9**, 270–304.

Druyan, L., Shah, K., Lo, K.-W., Marengo, J., and Russell, G.: 1995, 'Impacts of Model Improvements on GCM Sensitivity to SST Forcing', *Int. J. Clim.* **15**, 1061–1086.

Gates, L.: 1992, 'AMIP: The Atmospheric Model Intercomparison Project', *Bull. Amer. Meteor. Soc.* **73**, 1962–1970.

Handler, P.: 1984, 'Corn Yields in the United States and Sea-Surface Temperature Anomalies in the Equatorial Pacific Ocean during the Period 1868–1982', *Agric. For. Meteorol.* **31**, 25–32.

Hansen, J., Russell, G., Rind, D., Stone, P., Lacis, A., Lebedeff, S., Ruedy, R., and Travis, L.: 1983, 'Efficient Three-Dimensional Global Models for Climate Studies: Models I and II', *Mon. Wea. Rev.* **111**, 609–662.

Hansen, Sato, Ruedy, Lacis, Asamoah, Beckford, Borenstein, Brown, Cairns, Carlson, Curran, de Castro, Druyan, Etwarrow, Ferede, Fox, Gaffen, Glascoe, Gordon, Hollandsworth, Jiang, Johnson, Lawrence, Lean, Lerner, Lo, Logan, Luckett, McCormick, McPeters, Miller, Minnis, Ramberran, Russell, G., Russell, P., Stone, Tegen, Thomas, Thomason, Thompson, Wilder, Willson, and Zawodny: 1997, 'Forcings and Chaos in Interannual to Decadal Climate Change', *JGR* **102**, 25679–25720.

Hartke, G. and Rind, D.: 1997, 'Improved Surface and Boundary Layer Models for the GISS GCM', *JGR* **102**, 16407–16422.

Hastenrath. S. and Heller, L.: 1977, 'Dynamics of Climate Hazards in Northeast Brazil', *Quart. J. Roy. Meteorol. Soc.* **103**, 77–92.

Hastenrath, S. and Druyan, L.: 1993, 'Circulation Anomaly Mechanisms in the Tropical Atlantic Sector During the Northeast Brazil Rainy Season: Results from the GISS GCM', *J. Geophys. Res.* **98** (D8), 14917–14923.

Hastenrath, S. and Greischar, L.: 1993a, 'Circulation Mechanisms Related to Northeast Brazil Rainfall Anomalies', *J. Geophys. Res.* **98** (D8), 5093–5102.

Hastenrath, S. and Greischar, L.: 1993b, 'Further Work on the Prediction of Northeast Brazil Rainfall Anomalies', *J. Climate* **6**, 743–758.

Hoerling, M. and Kumar, A.: 1997, 'Origins of Extreme Climate States during the 1982–1983 ENSO Winter', *J. Climate* **10**, 2859–2870.

Houghton, J., Meira Filho, L., Callender, B., Harris, N., Kattenberg, A., and Maskell, K. (eds.): 1996, *Climate Change 1995: The Science of Climate Change*, Cambridge University Press, Cambridge, p. 250.

Kousky, V. and Chu, P-S.: 1978, 'Fluctuations in Annual Rainfall for Northeast Brazil', *J. Meteorol. Soc. Japan* **57**, 457–465.

Kousky, V. and Leetmaa, A.: 1989, 'The 1986–1987 Pacific Warm Episode: Evolution of Oceanic and Atmospheric Fields', *J. Climate* **2**, 254–267.

Lau, K.-M., Kin, J. H., and Sud, Y.: 1996, 'Intercomparison of Hydrologic Process in AMIP GCMs', *Bull. Amer. Meteorol. Soc.* **77**, 2209–2227.

Legates, D. and Willmott, C.: 1990, 'Mean Seasonal and Spatial Variability in Gauge-Corrected, Global Precipitation', *Int. J. Clim.* **10**, 111–127.

Lindesay, J.: 1988, 'South African Rainfall, the Southern Oscillation and a Southern Hemisphere Semi-Annual Cycle', *J. Climatol.* **8**, 17–30.

Makarau, A. and Jury, M.: 1997, 'Seasonal Cycle of Convective Spells over Southern Africa during Austral Summer', *Int. J. Clim.* **17**, 1317–1332.

Marengo, J. and Hastenrath, S.: 1993, 'Case Studies of Extreme Climatic Events in the Amazon Basin', *J. Climate* **6**, 617–627.

Matarira, C.: 1990, 'Drought over Zimbabwe in a Regional and Global Context', *Int. J. Clim.* **10**, 609–625.

Mechoso, C. and Lyons, S.: 1988, 'On the Atmospheric Response to SST Anomalies Associated with the Atlantic Warm Event during 1984', *J. Climate* **1**, 422–428.

Mechoso, C., Lyons, S., and Spahr, J.: 1990, 'The Impact of Sea-Surface Temperature Anomalies on the Rainfall over Northeast Brazil', *J. Climate* **3**, 812–826.

Moura, A. and Shukla, J.: 1981, 'On the Dynamics of Droughts in Northeast Brazil: Observations, Theory and Numerical Experiments with a General Circulation Model', *J. Atmos. Sci.* **38**, 2653–2675.

Reynolds, R. and Smith, T.: 1994, 'Improved Global Sea-Surface Temperature Analyses', *J. Climate* **7**, 929–948.

Rind, D. and Lerner, J.: 1996, 'Use of On-Line Tracers as a Diagnostic Tool in General Circulation Model Development. 1. Horizontal and Vertical Transport in the Troposphere', *JGR* **101**, 12667–12683.

Rind, D., Lerner, J., Shah, K., and Suozzo, R.: 1999, 'Use of On-Line Tracers as a Diagnostic Tool in General Circulation Model Development. 2. Transport between the Troposphere and Stratosphere', *JGR* **104**, 9151–9168.

Ropelewski, C. and Halpert, M.: 1987, 'Global and Regional Scale Precipitation Patterns Associated with El Niño/Southern Oscillation', *Mon. Wea. Rev.* **115**, 1606–1626.

Rosenzweig, C. and Abramopolous, F.: 1997, 'Land-Surface Model Development for the GISS GCM', *J. Climate* **10**, 2040–2054.

Rossow, W. and Schiffer, R.: 1991, 'ISCCP Cloud Data Products', *Bull. Amer. Meteorol. Soc.* **72**, 2–20.

Shah, K. and Rind, D.: 1995, 'Use of Microwave Brightness Temperatures with a General Circulation Model', *JGR* **100**, 13841–13874.

Shah, K. and Rind, D.: 1998, 'Comparison of Upper Tropospheric and Lower Stratospheric Temperatures: MSU, Radiosonde, CIRA and NCEP/NCAR Reanalysis Climatologies', *JGR* **103**, 31569–31591.

Shah, K., Rind, D., and Lonergan, P.: 1996, 'Could High-Speed Civil Transport Aircraft Impact Stratospheric and Tropospheric Temperatures Measured by Microwave Sounding Unit?', *JGR* **101**, 28711–28721.

Spencer, R. and Christy, J.: 1992, 'Precision and Radiosonde Validation of Satellite Gridpoint Temperature Anomalies', *J. Climate* **5**, 847–857.

Uvo, C., Repelli, C., Zebiak, S., and Kushnir, Y.: 1998, 'The Relationships between Tropical Pacific and Atlantic SST and Northeast Brazil Monthly Precipitation', *J. Climate* **11**, 551–562.

Ward, M. and Folland, C.: 1991, 'Prediction of Seasonal Rainfall in the North Nordeste of Brazil Using Eigenvectors of SST', *Int. J. Clim.* **11**, 771–743.

Yulaeva, A. and Wallace, J.: 1994, 'The Signature of ENSO in Global Temperature and Precipitation Fields Derived from the Microwave Sounding Unit', *J. Climate* **7**, 1719–1736.

(Received 16 June 1998; in revised form 7 May 1999)